

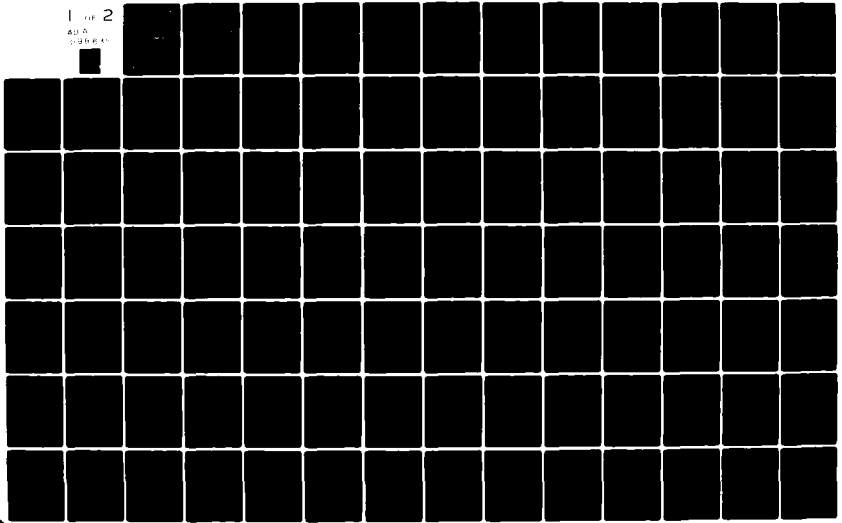
AD-A098 635

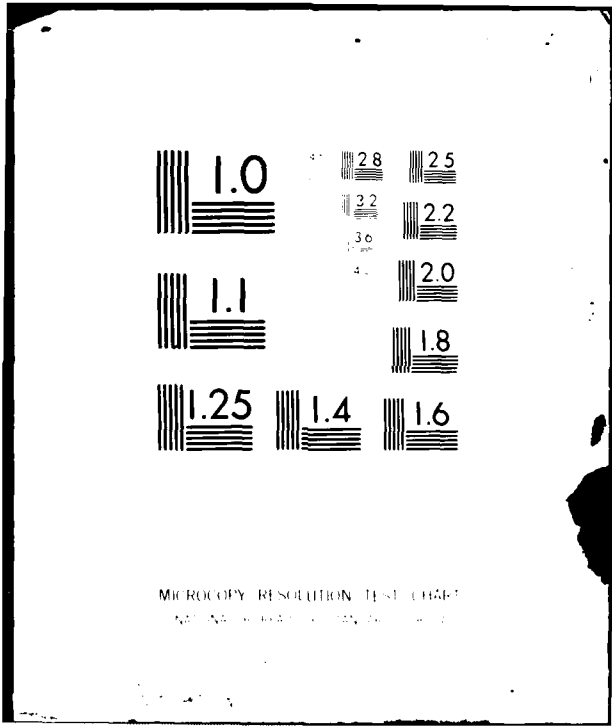
JAYCOR ALEXANDRIA VA
DEVELOPMENT OF A PBL PARAMETERIZATION SCHEME FOR THE TROPICAL C--ETC(U)
MAR 81 S W CHANG, C AGRITELLIS
JAYCOR-PSD-200-81-004FR

F/G 4/2
N00173-79-C-0465
NL

UNCLASSIFIED

1 of 2
AD-A098 635





MICROCOPY RESOLUTION TEST CHART
NBS 1963-A

AD A 098635

LEVEL *II*

②
SC

JAYCOR

DTIC
MAY 1981

DTIC FILE COPY

DISTRIBUTION STATEMENT A
Approved for public release;
Distribution Unlimited

8 3 31 042

300 Unicorn Park Drive
Woburn, Massachusetts 01801

2

6 DEVELOPMENT OF A PBL PARAMETERIZATION SCHEME FOR THE TROPICAL CYCLONE MODEL AND AN IMPROVED MAGNETOSPHERIC MODEL FOR MAGIC.

9 Final Rpt. 7 Sep 79 - 8 Sep 79

10 Simon Wei-jen / Chang
C. J. Pitelllis /

JAYCOR Project 6182

DTIC ELECTED
MAY 7 1981

Final Report on NRL

Contract No. N00173-79-C-0465

15

14 JAYCOR - PSD-200-81-004FR

11 25 Mar 1981

12 119

Submitted to:

Naval Research Laboratory
Washington, DC

DISTRIBUTION STATEMENT A
Approved for public release
Distribution unlimited

2939

UNCLASSIFIED

SECURITY CLASSIFICATION OF THIS PAGE (When Data Entered)

REPORT DOCUMENTATION PAGE		READ INSTRUCTIONS BEFORE COMPLETING FORM
1. REPORT NUMBER PDS-200-81-004FR ✓	2. GOVT ACCESSION NO. AD-A098635	3. RECIPIENT'S CATALOG NUMBER
4. TITLE (and Subtitle) DEVELOPMENT OF A PBL PARAMETERIZATION SCHEME FOR THE TROPICAL CYCLONE MODEL AND AN IMPROVED MAGNETOSPHERIC MODEL FOR MAGIC		5. TYPE OF REPORT & PERIOD COVERED Final Report 9/07/79 - 9/08/80
		6. PERFORMING ORG. REPORT NUMBER PSD-200-81-004FR
7. AUTHOR(s) S. Chang C. Agritellis		8. CONTRACT OR GRANT NUMBER(s) N00173-79-C-0465
		10. PROGRAM ELEMENT, PROJECT, TASK AREA & WORK UNIT NUMBERS
9. PERFORMING ORGANIZATION NAME AND ADDRESS JAYCOR ✓ 205 South Whiting St. Alexandria, VA 22304		12. REPORT DATE March 25, 1981
11. CONTROLLING OFFICE NAME AND ADDRESS Naval Research Laboratory Washington, DC 20375		13. NUMBER OF PAGES 116
14. MONITORING AGENCY NAME & ADDRESS (if different from Controlling Office) Same as block 11		15. SECURITY CLASS. (of this report) UNCLASSIFIED
16. DISTRIBUTION STATEMENT (of this Report) Code 4780 Code 4701 Code 4702 DDC Cameron Station		15a. DECLASSIFICATION/DOWNGRADING SCHEDULE
17. DISTRIBUTION STATEMENT (of the abstract entered in Block 20, if different from Report)		
18. SUPPLEMENTARY NOTES		
19. KEY WORDS (Continue on reverse side if necessary and identify by block number) Tropical Cyclone Model Generalized Similarity Theory Marine Winds Sea-Surface Temperature Planetary Boundary Layer		
20. ABSTRACT (Continue on reverse side if necessary and identify by block number) Reviewed are techniques and tools examined to improve the forecast ability of NRL's tropical cyclone model. Specifically considered are the impact of using satellite-sensed winds for forecast improvement, the effect of sea-surface temperature distribution and the utility of incorporating the planetary boundary layer.		

DISTRIBUTION STATEMENT A
 Approved for public release:
 Distribution Unlimited

TABLE OF CONTENTS :

	<u>Page</u>
Research Summary.	1
Appendix A	
"The Impact of Satellite-Sensed Winds On Intensity Forecasts of Tropical Cyclones"	
Appendix B	
"Numerical Simulation of the Influence of Sea-Surface Temperature on Translating Tropical Cyclones"	
Appendix C	
"Test of a Planetary Boundary Layer Parameterization Based on a Generalized Similarity Theory in Tropical Cyclone Models"	

Accession For	
NTIS GRA&I	<input checked="" type="checkbox"/>
DTIC TAB	<input type="checkbox"/>
Unannounced	<input type="checkbox"/>
Justification	
By	
Distribution /	
Avail. Statement	
Availability	
Dist	Special
A	

RESEARCH SUMMARY

The work performed under this contract has had a significant impact on existing abilities to predict the behavior of tropical cyclones and on abilities to model the predicted behavior of high altitude nuclear explosions (HANEs). This work has resulted in the generation of four pertinent publications, each of which is described below and attached as an appendix.

In "The Impact of Satellite-Sensed Winds on Intensity Forecasts of Tropical Cyclones", it is indicated that assimilation of these winds with marine surface (or low-level) wind alone does not improve intensity forecasts appreciably. A strong relaxation coefficient in the initialization scheme causes model rejection of the assimilation and an attenuating relaxation coefficient is recommended. However, when wind observations at the outflow level are included in the assimilation, forecasts improve substantially and the best forecasts are achieved when observations over the entire lower troposphere are assimilated.

In "Numerical Simulation of the Influence of Sea-Surface Temperature on Translating Tropical Cyclones", it is suggested that the sea-surface temperature distribution not only affects the intensity and path of tropical cyclones frictionally, but also thermally. The enhanced evaporation and convergence over the warm SST provide a favorable condition for the growth of the tropical cyclone, and leads to a gradual shift of the storm center toward the warm ocean.

"Test of a Planetary Boundary Layer Parameterization Based on a Generalized Similarity Theory in Tropical Cyclone Models", shows that in

comparison with a complex, one-dimensional, multi-layer PBL model, the GST parameterization yields accurate moisture fluxes, but slightly overestimates the momentum flux and underestimates the sensible heat flux. The GST parameterization produces very realistic dynamics, energetics and thermal structure in an axisymmetric tropical cyclone model.

In the HANE phenomenology portion of this research effort, considerable effort was devoted to enhancing and improving the capability of the PHARO simulation code. These improvements, as code modifications, have been delivered to NRL and are now integrated into PHARO. Another portion of this effort led to a unique interpretation of photographic data acquired on the STARFISH high altitude nuclear event and this work is being published separately as an NRL Memo Report because it is classified. The title of this report will be "Interpretation of High Altitude Streaks in Starfish (U), authored by S. Brecht, C. Agritellis, E. Hyman and P. Palmadesso. The report will be published at the Confidential level.

APPENDIX A

THE IMPACT OF SATELLITE-SENSED WINDS
ON
INTENSITY FORECASTS OF TROPICAL CYCLONES

JAYCOR

THE IMPACT OF
SATELLITE-SENSED WINDS ON
INTENSITY FORECASTS OF
TROPICAL CYCLONES

August 1980

Simon Wei-jen Chang

JAYCOR
205 South Whiting Street
Alexandria, VA 22304

TABLE OF CONTENTS

	Page
ABSTRACT.	1
1. Introduction.	2
2. Numerical Model	4
3. Experimental Design	6
4. Method of Assimilation.	10
5. Standard Forecasts.	13
6. Forecasts with Assimilation of Low-level Winds.	15
7. Forecasts with Assimilation of Low and Higher-level Winds	17
8. Deterioration of Forecast due to Satellite Observation Errors.	19
9. Summary and Discussion.	22
Acknowledgements.	24
References.	25
List of Figures	29

ABSTRACT

The impact of the satellite-sensed winds on the intensity forecasts of tropical cyclones is evaluated by a simulation study with an axisymmetric numerical model. The parameterized physics in the forecast model are deliberately made different from those in the model that generates the observation. Model generated "observations" are assimilated into forecasts by 12 h dynamic initialization.

A series of 24 h forecasts with and without assimilation of satellite-sensed winds are conducted and compared with the observations. Results indicate that assimilation with marine surface (or low-level) wind alone does not improve intensity forecasts appreciably, that a strong relaxation coefficient in the initialization scheme causes model rejection of the assimilation, and that an attenuating relaxation coefficient is recommended. However, when wind observations at the outflow level are included in the assimilation, forecasts improve substantially. The best forecasts are achieved when observations over the entire lower troposphere are assimilated.

Additional experiments indicate the errors in the satellite observations contaminate the forecast. But the assimilation of inflow and outflow winds still improve the intensity forecast if the satellite observation errors are less than or about the same magnitude of those in the initial wind field.

1. Introduction

The improvement of forecast skill in tropical cyclones evident in the 1960's has not been continued in the 1970's in spite of improved technology and continuing effort. The lack of improvement has been attributed to the imperfect knowledge of the initial fields for objective models. Elsberry (1977) attributed the poor performance of his prediction model to the deficiency of the initial wind data. For the 1976 Atlantic tropical cyclone season, Hovermale and Livezey (1977) showed the errors for the 36- and 48-h track forecasts increased by approximately a factor of three for storms over data-void ocean regions as compared to storms near coastal stations. In addition, the theory of geostrophic adjustment requires that the mass field adjusts to the momentum field for low latitudes and tropical cyclone scales of motion. (Monin and Obukhov, 1959; Washington, 1964). It is beyond doubt that wind observations are essential to tropical cyclone forecasts.

Although initial wind analyses of tropical cyclones have been improved from reconnaissance aircraft flights, the quantity and especially the aerial coverage of wind data so obtained are inadequate for numerical model initializations. Remote measurements from geostationary and orbiting satellites will be relied upon as important data sources. Rodgers et al (1979) explained techniques to derive low-level and outflow level winds for tropical cyclones by tracking clouds using successive satellite images. Their results are encouraging in spite of some difficulties such as the short lives of cloud turrets and overcast conditions near the storm centers. An experimental oceanographic satellite known as SEASAT-1 during its short

lifetime provided an additional data source to define large and mesoscale wind fields near tropical cyclones. A special scatterometer (SASS) flown with SEASAT-1 measured the marine surface microstructures and, through appropriate algorithms, marine surface winds were inferred.

The purpose of this study is to evaluate the impact of the satellite-sensed winds on tropical cyclone intensity forecasts. As a simulation study, data generated by numerical models will be used in place of real data. The general strategy of such simulation studies follows that of Charney et al (1969). First, a control integration of the numerical forecast model is performed to generate the "true" history of the atmosphere or the "observation". A series of "standard forecasts" is then generated based on different initial states. Finally, a series of forecasts with the "observations" assimilated are conducted to evaluate the impact of assimilation. For detailed reviews of such simulation studies and their general strategies, readers are referred to McPherson (1975) and Bengtsson (1975).

As a preliminary study, an axisymmetric tropical cyclone model is employed in this study, therefore only the impact on intensity can be studied. The method of assimilation used is the dynamic initialization by relaxation (DIR) technique. To approximate the relationship between the real atmosphere and forecast models, parameterized physics in the model that generates forecasts (forecast model) are altered from those in the model that generate the observations (natural model). In the following sections, the numerical model, the experimental design, and the method of assimilation will be discussed in sequence. Finally, the results, conclusions and proposed future research will be presented.

2. Numerical Model

The axisymmetric tropical cyclone model used in this study is similar to the one described in Chang (1977) and Anthes and Chang (1978). The governing equations are in primitive form and are in $\sigma (=P/P_s)$ coordinates. The explicit water vapor cycle and parameterization of cumulus convection follows Kuo (1974) and Anthes (1977). The boundary layer is contained in the lowest model layer and parameterization of various vertical fluxes is based on a generalized similarity theory in which Yamada's (1975) universal functions are used (Chang, 1980). Charnock's equation is applied to compute marine surface roughness length.

The model atmosphere is divided into six layers (Table 1). A uniform horizontal grid interval of 30 km is used from the center to a radius of 600 km. The grid interval is progressively increased by a factor of two outside 600 km. The leapfrog temporal integration method with the time-averaged pressure gradient force (Brown and Campana, 1978) is employed for numerical integration. The spatial finite differencing is of the second order. The mean hurricane season sounding (Sheets, 1969) is used for the initial and lateral boundary conditions. The coriolis parameter f has the constant value $5 \times 10^{-5} \text{ s}^{-1}$.

A period of 36 h of the control run during which the model tropical cyclone undergoes a rapid intensification is chosen as the "truth" or "observation" (thereafter referred to as such in this study except as stated otherwise). For convenience, -12 h and 24 h are designated as the start and end of this period. We selected a period of rapid intensification for study in order to magnify errors in the forecasts.

Table 1. Vertical Structure of the Model

Layer	$\Delta P(\text{mb})$ for $P_s = 1000$	Undisturbed Height (km) at Layer Center
1	0 - 200	18.3
2	200 - 300	10.6
3	300 - 600	6.7
4	600 - 800	3.0
5	800 - 930	1.2
6	930 - 1000	0.3

3. Experimental Design

In recent years, many simulation studies have been conducted to evaluate the impact of incomplete observation data on numerical predictions (e.g., Charney et al, 1969; Kasahara and Williamson, 1972; Morel and Talagrand, 1974; Anthes, 1974; Cane et al, 1979). In a similar manner, numerical integrations conducted for this study can be grouped into three components (Table 2):

- (1) Nature run - A 36 h segment of life history of tropical cyclones designated as observation as defined in Section 2.
- (2) Standard forecasts - A 36 h forecast starting from - 12 h and a 24 h forecast starting from 0 h. The initial conditions for standard forecasts are obtained by the static, non-divergent initialization method based on the nature run.
- (3) Forecasts with assimilation - 12 h preforecast integrations starting from -12 h, during which satellite-sensed winds are assimilated into the model solution followed by 24 h forecasts starting from 0 h.

A unique characteristic of previous simulation studies is that a prediction model will make an error-free forecast given error-free model-generated initial conditions (Williamson, 1973). Because this is rather unrealistic, errors of various kinds were added to the observations either in initial conditions for the forecasts, or in data for assimilation. Both random errors (e.g., Williamson and Kasahara, 1971) and bias errors (e.g., Anthes, 1974) have been introduced into the observations in previous studies. Forecast runs with initial random errors sometimes exhibit

Table 2. List of Simulation Experiments

Components	Experiments	Total length of Integration	Assimilation Period (h)	Observations Assimilated	Relaxation Coefficient
Nature	1	-12 to 24	Observation		
Forecasts	2	-12 to 24	Standard 36 h forecast		
	3	0 to 24	Standard 24 h forecast		
Forecasts with low-level wind observations assimilated	4	-12 to 24	-12 to 0	u_6, v_6^*	Weak
	5	-12 to 24	-12 to 0	u_6, v_6	Strong
	6	-12 to 24	-12 to 0	u_6, v_6	Attenuating
Forecasts with low- and higher-level wind observations assimilated	7	-12 to 24	-12 to 0	v_5, u_6, v_6	Attenuating
	8	-12 to 24	-12 to 0	v_4, v_5, u_6, v_6	Attenuating
	9	-12 to 24	-12 to 0	u_2, v_2, u_6, v_6	Attenuating
Forecasts with low and outflow winds containing errors assimilated	9E	-12 to 24	-12 to 0	u_2, v_2, u_6, v_6	Attenuating
	9E2	-12 to 24	-12 to 0	u_2, v_2, u_6, v_6	Attenuating

* u, v are radial and tangential winds, respectively. Subscripts denote layers.

unrealistic error growth characteristics because gravity waves and model physics act to smooth them. Besides, random observational errors are not the major problem with real data, where systematic errors are known to have caused more problems (McPherson, 1975). Biased errors are generally determined subjectively and may be unwarranted and unrealistic. No error is artificially added in the initial fields for all forecast runs in our study, instead, errors in the initial wind fields are introduced by the non-divergent, gradient-balanced, static initialization procedure adopted here. Such initialization procedure is currently in use operationally. Figure 1 shows the errors of speed in the initial wind fields of forecasts at -12 h. As expected, large errors occur in the low-level and the outflow level, where divergent components of wind vectors are largest. The initial errors for forecasts initialized at 0 h have the same characteristics.

In previous simulation studies, the models which generated the forecasts were identical with the models that generated the observations (see McPherson, 1975, for review). This, of course, is very unrealistic. In reality, numerical forecasting models with finite spatial resolutions and parameterized physics cannot reproduce the atmosphere even if perfect initial conditions are obtained. To properly account for the discrepancies between real forecasting models and the atmosphere, the parameterized physics in our forecast model are deliberately altered. The parameters changed are those we feel most uncertain about in the physical parameterizations in current numerical models, namely, the effective air-sea exchange coefficients and the vertical distribution of latent heat. The effective coefficients of

eddy transfers of momentum, sensible heat and latent heat in the forecast model are set at 90% of those in the nature model. The 10% error is well within the expected error in the boundary layer formulations. The vertical distribution of cumulus heating is also changed so that approximately 5% of the heating in the lower troposphere is shifted to upper troposphere. The 5% difference is within the variation of the observed heating distributions. Due to these two changes, the forecasts in our study do not asymptotically approach the observations even after long integration. Because the errors in the parameterized physics in our forecast model are within the differences between the atmosphere and the current operational forecast models, the asymptotic difference between our "forecasts" and "observation" is quite realistic.

4. Method of Assimilation

The satellite-sensed data are in many occasions incomplete in that they do not contain observations of all meteorological variables simultaneously or the observations are made at different locations and times. To incorporate such data in a dynamically consistent way into the numerical models, suitable methods of assimilation must be used. From the direct insertion method (e.g., Charney et al, 1969) to the complicated variational assimilation (e.g., Sasaki, 1969), there are many methods of assimilation in existence. However, not all methods are applicable for the satellite-sensed data in question. The wind fields derived from GOES images are basically restricted to low and outflow-levels in tropical cyclones (Rodgers et al, 1979), and wind fields measured from SEASAT-1 are at anemometer level. For such data with poor vertical resolution, a method called dynamic initialization by relaxation (DIR) is desirable.

DIR is a technique wherein the meteorological variables are relaxed (or nudged) by using the model's governing equations toward the observed values during a preforecast integration (Anthes, 1974; Hoke and Anthes, 1976). The technique has shown great promise in real data applications (Nitta and Hovermale, 1969; Davies and Turner, 1977; Hoke and Anthes, 1977). Mathematically, governing equations during the preforecast integration are modified to:

$$\frac{\partial x}{\partial t} = F(\underline{X}, t) + \sum_{n=1}^N \lambda(\epsilon_n, \delta t, \delta r, \delta z) (x^0 - x) \quad (1)$$

where x is an element in the vector of variables \underline{X} , the function F contains the normal terms in governing equations, x^0 is the observation, N the number

of observations, and λ the relaxation coefficient. In a full four dimensional assimilation, λ is the function of observational error, ϵ_n , the time separation of the observation, δt , the horizontal, (δr) , and the vertical, (δz) , spatial separations between observations and grid points. It should also depend on the meteorological variables.

To simplify the functional form of λ , we will use point-to-point relaxation, i.e., variables are relaxed toward observations made at the same model grid points only. This requires that observations be taken at model grid points and all observations be taken simultaneously. Note that the horizontal resolution of the satellite measurements does approach those of typical operational forecast model of tropical cyclones. With the development of suitable boundary layer models for vertical extrapolation (Yu, 1980), the convenience of point-to-point relaxation assumed for convenience in this study is nearly available in operational forecasting. The time lag of measurements over the domain of tropical cyclones within one satellite revolution is negligibly short as compared to the 12-h preforecast integration. We take note that the swath width of orbiting satellites nevertheless may not be large enough to cover the entire tropical cyclone.

The satellite-sensed winds are not free of errors. Rodgers et al (1979) estimated the mean speed errors in their derived winds to be 2.5 m s^{-1} relative to aircraft measurements. There are conflicting reports on the errors of SEASAT measurements (Black, 1979; Jones and Pierson, 1978), but, in general, the errors of satellite-sensed winds are smaller than those introduced by the objective analyses over the oceans (Cardone et al, 1976). The contribution of satellite measurements is not

in the general error reduction but in the filling of data-void areas (Ghil et al, 1979). For a clear demonstration of the impact in assimilating winds at different levels, in Exps. 2-9 it is justifiable to assume that the satellite observations are error-free in comparison to the initial and model errors. However, errors of different magnitudes are added to the satellite-sensed wind in Exps. 9E and 9E2 to evaluate the extent to which the observation errors contaminate the forecast.

The equations of motion in the preforecast integration in this study can simply be written

$$\frac{\partial}{\partial t} \underline{v}_k = F(\underline{x}, t) + \lambda(\underline{v}_k^0 - \underline{v}_k) \quad (2)$$

where k denotes the layer in the model where observations are available. Three different values for λ are tested: $\lambda_w = 10^{-4} \text{ s}^{-1}$ for weak relaxation, $\lambda_s = 10^{-3} \text{ s}^{-1}$ for strong relaxation; and $\lambda_a = \lambda_s (\delta t - t)/12$, $-12 \text{ h} \leq \delta t \leq 0$ for attenuating relaxation. Figure 2 illustrates the time variations of λ . Observations are assumed to be taken at 0 h and are assimilated into model prediction during -12 to 0 h in all of the assimilation experiments (Exps. 4 - 9).

in the general error reduction but in the filling of data-void areas (Ghil et al, 1979). For a clear demonstration of the impact in assimilating winds at different levels, in Exps. 2-9 it is justifiable to assume that the satellite observations are error-free in comparison to the initial and model errors. However, errors of different magnitudes are added to the satellite-sensed wind in Exps. 9E and 9E2 to evaluate the extent to which the observation errors contaminate the forecast.

The equations of motion in the preforecast integration in this study can simply be written

$$\frac{\partial}{\partial t} \underline{V}_k = F(\underline{X}, t) + \lambda(\underline{V}_k^0 - \underline{V}_k) \quad (2)$$

where k denotes the layer in the model where observations are available. Three different values for λ are tested: $\lambda_w = 10^{-4} \text{ s}^{-1}$ for weak relaxation, $\lambda_s = 10^{-3} \text{ s}^{-1}$ for strong relaxation; and $\lambda_a = \lambda_s (\delta t - t)/12$, $-12 \text{ h} \leq \delta t \leq 0$ for attenuating relaxation. Figure 2 illustrates the time variations of λ . Observations are assumed to be taken at 0 h and are assimilated into model prediction during -12 to 0 h in all of the assimilation experiments (Exps. 4 - 9).

5. Standard Forecasts

During the period between -12 h and 24 h, observation shows a rapid intensification of the tropical cyclone, the minimum central pressure deepens from 998 mb to 953 mb (Figure 3) and the maximum wind speed increases from 29 m s^{-1} to 52 m s^{-1} (Figure 4). A 36 h forecast starting from -12 h (Exp. 2) and a 24 h forecast starting from 0 h (Exp. 3) are conducted based on the error-free initial mass field and non-divergent, gradient-balanced wind fields. Typical wind speed errors in the initial wind field are illustrated in Figure 1.

As expected from previous experience, both forecasts have an initial dissipation stage due to the onset of the surface friction. The weakening of storm intensity is especially pronounced in Exp. 3 in that it has larger intensity errors before 12 h than Exp. 2 which is initialized 12 h earlier. This is indicative of the inadequacy of the static, non-divergent initialization employed. Improvement of forecast during the initial hours can be achieved by using a divergent static (Tarbell, 1979) or a dynamical (Hovermale and Livezey, 1977; Kurihara and Bender, 1979) initialization scheme.

After the radial circulations develop, both forecasts reproduce the observed intensification but at slower rates. After 12 h, the 24 h forecast (Exp. 3) yields better prediction than the 36-h forecast by approximately 2 mb in minimum pressure and 2 m s^{-1} in maximum wind speed. Both forecasts predict weaker storm intensity as compared to the observation. The difference between the observed and predicted intensities at 24 h is about 15 mb in minimum pressure and 10 m s^{-1} in maximum wind speed. The divergence of the forecasts from the observation is a consequence of the "imperfect"

physical parameterizations in the forecast model.

We selected the root-mean-square errors (\bar{e}) as a measurement of the accuracy of the predictions (Panofsky and Brier, 1968). Evolutions of \bar{e} for wind speed (V), temperature (T), and specific humidity (q) with respect to the observation for Exps. 2 and 3 are shown in Figures 5, 6, and 7, respectively. The initial $\bar{e}(V)$ is large at about 4 m s^{-1} in both experiments due to the non-divergent initialization. It decreases for the first 18 h in both experiments as the forecast storms intensify. As evident in Exp. 2 after 6 h, values of $\bar{e}(V)$ begins to increase, indicating a deteriorating forecast.

Both $\bar{e}(T)$ and $\bar{e}(q)$ increase rapidly after initialization with time from the error-free mass field. Their values escalate to 1.5°K in temperature and $0.9 \sim 1.1 \text{ g kg}^{-1}$ in specific humidity at 24 h. Here again, Exp. 3 produces a better prediction than Exp. 2 during most of the period 0 - 24 h.

6. Forecasts with Assimilation of Low-level Winds

In Exps. 4, 5, and 6, the observed low-level radial (u_0) and tangential (v_0) winds at 0 h are assimilated by DIR into the 24-h forecast during a preforecast integration from -12 to 0 h (Table 2). The relaxation coefficients are λ_w , λ_s , and λ_a in Exps. 4, 5, and 6, respectively (Figure 2).

Figures 8 and 9 show the minimum pressures and the maximum wind speeds for these three forecasts with low-level winds assimilated. It is apparent that the DIR with the weak relaxation coefficient (Exp. 4) does not alter the prediction appreciably toward the observation during the preforecast integration. The following 24 h forecast shows no apparent improvement over the standard forecasts.

The model adjustments are considerable when strong and attenuating relaxation coefficients are applied in Exps. 5 and 6. The maximum wind speed in the preforecast integration converges to the observed value within a couple of hours. The minimum pressure also approaches the observed value at 0 h within 6 h, in agreement with the theory of geostrophic adjustment. The maximum wind speed in Exp. 5 achieves the observed value due to constantly strong relaxation. However, as the assimilation terminates at 0 h, strong model adjustments occur in both experiments. The model rejection occurs in Exp. 5 where the maximum wind speed decreases approximately 5 m s^{-1} in three hours and stays lower than that of the standard forecast (Exp. 2). The rejection is similar in Exp. 6, so there is still no improvement in intensity forecast.

We thus conclude that low-level wind observations are not beneficial to intensity forecasts of tropical cyclones if assimilated by DIRT. We can also conclude that the attenuating relaxation coefficient λ_a is more effective in assimilating the observed data (cf. Fig. 9) and

desirable for eliminating model adjustments.

However, an examination of forecast errors in Exps. 4, 5, and 6 is warranted. During the preforecast integration, $\bar{e}(V)$ decreases with time as relaxation forces the low-level wind to asymptotically approach the 0 h observation. The $\bar{e}(V)$ value from Exp. 5 at 0 h reaches the lowest level of all (Figure 10). The model adjustments cause the error to be at levels higher than those of the standard forecasts (Exps. 2 and 3) after 6 h since the assimilation has been rejected by the model. The $\bar{e}(T)$ and $\bar{e}(q)$ are similar to $\bar{e}(V)$ in that they decrease with time in the preforecast integration for strong relaxation and they subsequently increase to levels equivalent or higher than those of the standard forecasts.

The rejection of assimilation of low-level winds in the preceding experiments can be attributed to the insufficient vertical coupling between the low-level and high-level momentum fields during the 12-h period of preforecast integration. A longer period of preforecast integration may produce enough vertical coupling through model dynamics and physics, but is not very meaningful in practice. It is then logical to test assimilation of additional wind observations at higher levels since they can be made available (Rodger et al, 1979).

7. Forecasts with Assimilation of Low and Higher-level Winds

As listed in Table 2, observations of higher level winds in addition to the low-level winds are assimilated by DIR using relaxation coefficient λ_a . In Exp. 7, v_5 (check Table 1 for pressure level) at 0 h is assimilated; in Exp. 8, v_4 and v_5 ; and in Exp. 9, u_2 and v_2 .

The assimilations of higher level winds yield significantly different intensity forecasts from the standard forecasts as evident in Figures 11 and 12 showing the minimum pressure and the maximum wind speed, respectively. In addition, the three experiments forecast very different minimum pressures even during the preforecast integration where the same λ_a is used. Among the three, Exp. 8 yields the best prediction, with maximum difference of only 4.5 mb in central pressure at 24 h. Exp. 7 predicts a very intense storm with central pressure deepening to 955 mb at 12 h. Exp. 9 predicts a weaker storm than the observation, however, it forecasts better than the standard forecasts (Exps. 2 and 3) and forecasts where only low-level winds are assimilated (Exps. 4, 5, and 6).

It is interesting that the storm intensities in Exps. 7 and 8 are drastically different when the only difference in the experiments is that the observations of v_4 at 0 h are available for assimilation in Exp. 8. As demonstrated by the vertical profile of v at $r = 30$ km in Figure 13, there is a strong vertical shear in the 0 h tangential wind observation. Tangential wind speed decreases upward associated with the strong warm core at level 4. In Exp. 7, the too strong storm intensity is due to the assimilation of the stronger circulation below 800 mb, whereas the vertically decreasing tangential circulation and effects of warm core are properly assimilated in Exp. 8. This suggests that when observational data are to be vertically

interpolated in diagnosis or analysis, strong vertical shear and the related baroclinic effect must be taken into account.

The forecast errors in wind speed, temperature and water vapor are shown in Figures 14, 15, and 16, respectively. The values of $\bar{e}(V)$ decrease in time during the preforecast integration as in Exps. 4, 5, and 6. Note the $\bar{e}(V)$ in Exp. 9 is the smallest because initial errors are largest at the assimilated levels (Figure 1). The errors in Exps. 8 and 9 remain smaller than those of the standard forecasts, especially in Exp. 9, where the error is 50% lower.

The error in temperature field of Exp. 7 arises early in the preforecast integration. This shows that the effects of the warm core on tangential circulation are not properly assimilated as mentioned earlier. The errors in Exps. 8 and 9 are generally smaller than for the standard forecasts throughout the 24 h forecast period. The specific humidity errors for these three forecast experiments are higher than for the standard forecasts with Exp. 7 having the highest error. Between -12 and 6 h, $\bar{e}(q)$ in Exp. 8 is very low because the inflow and outflow, which nearly determine the net total water vapor convergence, are assimilated.

The higher $\bar{e}(q)$ in Exps. 8 and 9, in spite of the better intensity forecasts and lower $\bar{e}(V)$ and $\bar{e}(T)$, is probably due to the different physical parameterizations in the forecast model.

8. Deterioration of Forecast due to Satellite Observation Errors

In previous sections, we have examined the impact of assimilating the error-free satellite winds. The assumption of perfect satellite observation is for clarity in comparison. Satellite-sensed winds are, of course, not error-free. As discussed earlier, the mean speed error in satellite winds varies from 2.5 m s^{-1} (Rodgers *et al.*, 1979) to as large as 8 m s^{-1} (Black, 1979). We now turn our attention to the influence of the satellite observation errors on the forecast.

Because low- and outflow-level winds are most likely to be obtainable operationally, we repeat Exp. 9 with artificially introduced observation errors in both the initial condition and satellite-sensed winds. Randomized error of about 2.5 m s^{-1} and biased errors are added into the observation at -12 h. The biased errors have a maximum of 8 m s^{-1} at $r = 30 \text{ km}$, decreasing with radius to zero at $r = 150 \text{ km}$. These errors, after the balanced, static initializations, are equivalent to approximately 0.5°K errors in the temperature field and a 4 mb error in central pressure. Four experiments, Exps. 2E, 3E, 9E, and 9E2, are carried out based on initial conditions containing such errors. The satellite-sensed winds at 0 h contain random errors with maximum speed error of 2.5 m s^{-1} in Exp. 9E and 5 m s^{-1} in Exp. 9E2. Exps. 2E and 3E are identical to Exps. 2 and 3 except for the introduced errors in the initial condition.

As summarized in Table 3, the average 12- and 24-h forecasts in Exps. 2E, 3E, and 9E are worse than their respective counterparts in error-free simulations. For example, Exp. 9 has an averaged forecast error of 11 mb in minimum pressure, 6.5 m s^{-1} in maximum wind speed, and 2.5 m s^{-1} in $\bar{e}(V)$, whereas Exp. 9E has an averaged forecast error of 16 mb, 11.7 m s^{-1} , and 4.5 m s^{-1} . It is encouraging that Exp. 9E, in which the magnitude of the

Table 3. 12 and 24 h Averaged Forecast Errors

Experiment	Initial $\bar{e}(V)$ ($m\ s^{-1}$)	Magnitude of Satellite Obs. Error ($m\ s^{-1}$)	12 and 24 h Forecast Errors			
			Min. P. (mb)	Max Wind ($m\ s^{-1}$)	$\bar{e}(V)$ ($m\ s^{-1}$)	$\bar{e}(T)$ OK
2	~4	--	15	8.5	3.2	1.18
3	~4	--	13	7.2	3.1	1.09
9	~4	0	11	6.5	2.5	0.95
2E	~5	--	21	13.4	5.0	1.75
3E	~5	--	20	13.1	4.9	1.67
9E	~5	2.5	16	11.7	4.5	1.5
9E2	~5	5	17	11.8	4.6	1.5

observation errors are typical for operational forecasts, is a better forecast than the standard forecasts of Exps. 2E and 3E. It forecasts better than the standard forecasts by 4 mb in minimum pressure, approximately 2 m s^{-1} in maximum wind, and 0.5 in $\bar{e}(V)$. It is also interesting that Exp. 9E2 performs only slightly worse than Exp. 9E, although the error level is twice as large as that in Exp. 9E.

From the above comparison, we conclude that the errors in satellite winds could deteriorate a forecast, and that the assimilation of satellite low- and outflow-level winds can improve the forecast if these errors are less or equal to those contained in the initial wind field.

9. Summary and Discussion

The impact of accurately measured marine surface winds of sufficient spatial coverage and resolution in the 24 h intensity forecast of tropical cyclones has been studied with simulation experiments. The model physics in the forecast model were altered from those in the nature model. The observations are assimilated into the numerical forecast with dynamical initialization by relaxation during the preforecast integrations from error-free mass fields.

The results indicate no improvement in forecast accuracy when low-level winds are assimilated according to the abovementioned procedure. We note that a strong relaxation coefficient causes rejection of the assimilation within a few hours of forecasting and that a weak relaxation coefficient is ineffective.

Significant improvements are achieved when all winds below 600 mb are assimilated. This conclusion is easily understandable because the major characteristics of the tropical cyclone such as the vortex strength, the warm core, and the vertical shear are included in such observations. But simultaneous, high-resolution observations required for such assimilation are difficult to obtain. It is encouraging that forecast improvement can also be achieved when low-and outflow-level winds are assimilated because wind fields at these two levels are most likely available from satellite observations.

The forecast with low-and outflow-level winds assimilated worsens with increasing observation errors. However, even if the root-mean-square error in the satellite observation is equivalent to that in the initial wind field, assimilation of low-and outflow-level winds still improves the forecast.

Caution must be taken in interpreting these findings for operational applications, as is the case for all simulation studies, because the extent to which they approximate reality is difficult to determine. The finding that the low-level wind observations alone cannot improve the forecast when assimilated by DIR should not cast doubt on the usefulness of observing systems which measure marine surface winds. Since an axisymmetric tropical cyclone is employed in this study, the position of the storm is assumed known. Also, the mass fields are assumed to be error-free in the static initializations of the forecasts. The precise center location and perfect mass field are not commonly available for operational forecasts, where meteorologists have to be content with uncertainties of the storm center position and with the "bogussed" circulations. The marine surface winds are invaluable in defining the low-level circulations and in locating the storm centers which otherwise would be impossible over data-void oceans.

Since our results with assimilation of the low and outflow-winds are encouraging and since these will be the focal levels in satellite observations, future research with a three-dimensional tropical cyclone model is warranted. In a three-dimensional study, the impact of the satellite-sensed winds on storm track forecasts can be investigated. The effects of time-lag within one satellite revolution discussed earlier and the effects of the swath width can also be studied. Finally, real data case studies can be carried out with a three-dimensional model.

Acknowledgements

The author thanks Dr. Rangarao V. Madala for support and Mrs. Jane Polson for typing the manuscript. Drs. W. Chao, D. F. Strobel, M. R. Schoeberl, and R. T. Williams commented on the manuscript.

The research is supported by the Naval Research Laboratory through contract N00173-78-C-465.

REFERENCES

- Anthes, R. A., 1974: Data assimilation and initialization of hurricane prediction models. J. Atmos. Sci., 31, 702-719.
- Anthes, R. A., 1977: A cumulus parameterization scheme utilizing a one-dimensional cloud model. Mon. Wea. Rev., 105, 270-286.
- Anthes, R. A., and S. W. Chang 1978: Response of the hurricane boundary layer to changes of sea-surface temperature in a numerical model. J. Atmos. Sci., 35, 1240-1255.
- Bengtsson, L., 1975: Four-dimensional assimilation of meteorological observations. GARP publication series No. 15, Geneva, World Meteorological Organization, 76 pp.
- Black, P. G., 1979: SEASAT-derived surface wind fields in eastern Pacific Hurricane FICO. 12th Technical Conference on Hurricane and Tropical Meteorology, American Meteorological Society, April 24-27, 1979. New Orleans, LA.
- Brown, J. A., Jr., and K. A. Campana, 1978: An economical time-differencing system for numerical weather prediction. Mon. Wea. Rev., 106, 1125-1136.
- Cane, M. A., V. J. Cardone, M. Halem, I. Halberstram, and J. Ulrich, 1979: Observing systems simulation and potential impact of marine surface wind data on numerical weather prediction. Manuscript submitted to Mon. Wea. Rev.
- Cardone, V. J., J. D. Young, W. J. Pierson, R. K. Moore, J. A. Greenwood, C. Greenwood, A. K. Fung, A. Salfi, H. L. Chan, M. Afarani, and M. Komen, 1976: The measurement of the winds near the ocean surface

with a radiometer-scatterometer on Sky Lab. A joint meteorological, oceanographic, and sensor evaluation program for Experiment S193 on Skylab. NASA CR-147478.

Chang, S. W., 1977: The mutual response of the tropical cyclone and the ocean as revealed by an interacting atmospheric and oceanic model. Ph.D. Dissertation, Dept. of Meteorology, Pennsylvania State University, 210 pp. Available at University Microfilm International, Dissertation Copies, P. O. Box 1764, Ann Arbor, Michigan 48106. Order No. 77-23, 218.

Chang, S. W., 1980: Test of a planetary boundary layer parameterization based on generalized similarity theory in tropical cyclone models. Submitted to Mon. Wea. Rev.

Charney, J., M. Halem, and R. Jastrow, 1969: Use of incomplete historical data to infer the present state of the atmosphere. J. Atmos. Sci., 26, 1160 - 1163.

Davies, H. C., and R. E. Turner, 1977: Updating prediction models by dynamic relaxation: An examination of the technique. Quart. J. Roy. Meteor. Soc., 103, 225-245.

Elsberry, R. L., 1977: Operational data tests with a tropical cyclone model. Tech. Report NPS-63ES 77031, Naval Post Graduate School. 28 pp.

Ghil, M., M. Halem, and R. Atlas, 1979: Time-continuous assimilation of remote-sounding data and its effect on weather forecasting. Mon. Wea. Rev., 107 140-171.

Hoke, J. E., and R. A. Anthes, 1976: The initialization of numerical models by a dynamic-initialization technique. Mon. Wea. Rev., 104, 1551-1556.

- Hoke, J. E., and R. A. Anthes, 1977: Dynamic initialization of a three-dimensional primitive-equation model of Hurricane Alma of 1962. Mon. Wea. Rev., 105, 1211 - 1350.
- Hovermale, J. B., and R. E. Livezey, 1977: Three-year performance characteristics of the NMC hurricane model. Proc., 11th Technical Conf. on Hurricane and Tropical Meteorology, AMS, Miami Beach, FL. 122-125.
- Hovermale, J. B., and R. E. Livezey, 1977: Three-year performance characteristics of the NMC hurricane model. Post Print, 11th Technical Conf. on Hurricane and Tropical Meteorology, AMS, Miami Beach. FL.
- Jones, W. L., and W. J. Pierson, 1978: Preliminary evaluation of scatterometer winds from SEASAT-A. American Geophysical Union meeting, Dec. 4-8, 1978, San Francisco, CA.
- Kasahara, A., and D. Williamson, 1972: Evaluation of tropical wind and reference pressure measurements: Numerical experiments for observing systems. Tellus, 24, 100 - 115.
- Kuo, H. L., 1974: Further studies of the parameterization of the influence of cumulus convection on large-scale flow. J. Atmos. Sci., 31, 1232 - 1240.
- Kurihara, Y., and M. A. Bender, 1979: Supplementary note on "A scheme of dynamic initialization of the boundary layer in a primitive equation model." Mon. Wea. Rev., 107, 1219 - 1221.
- McPherson, R. D., 1975: Progress, problems, and prospects in meteorological data assimilation: Bull. Amer. Meteor. Soc., 56, 1154 - 1166.
- Monin, A., and A. Obukhov, 1959: A note on the general classification of motions in a baroclinic atmosphere. Tellus, 11, 159 - 162.

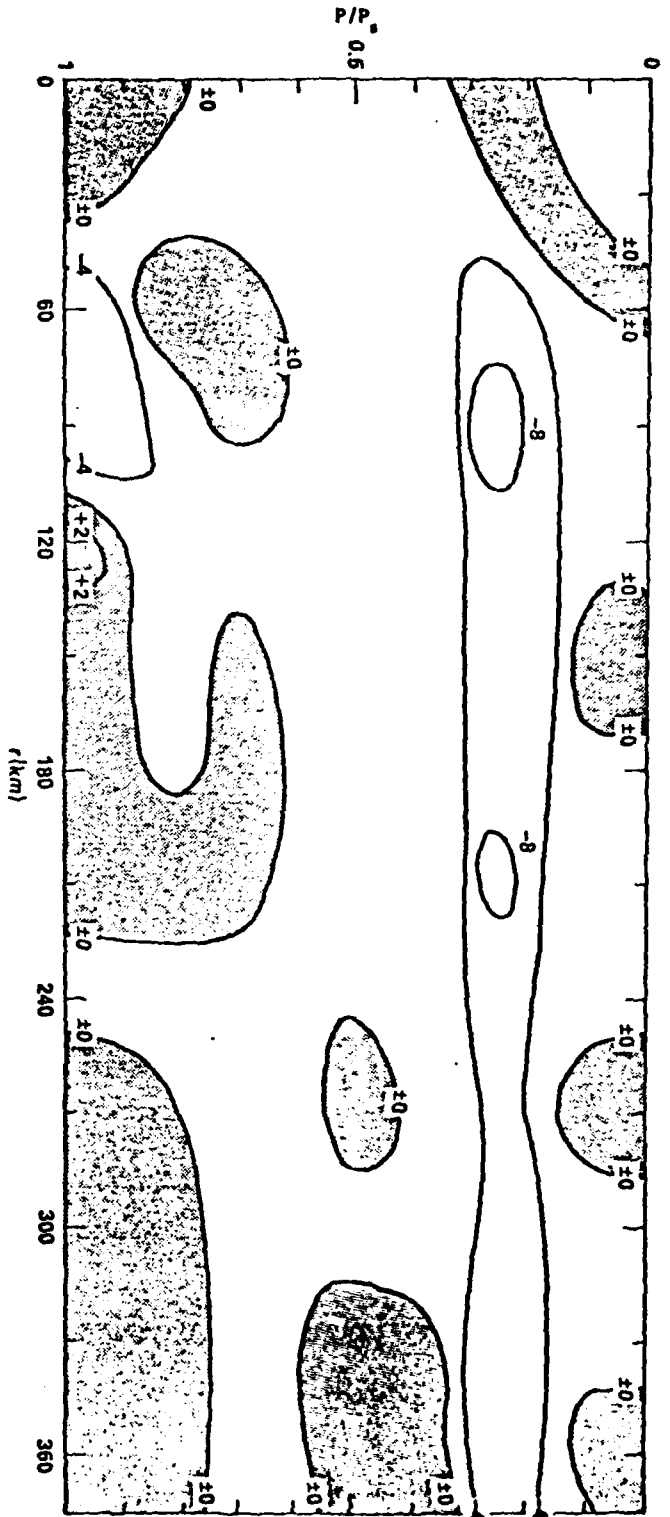
- Morel, P., and O. Talagrand, 1974: Dynamic approach to meteorological data assimilation. Tellus, 26, 334-343.
- Nitta, T., and J. B. Hovermale, 1969: A technique of objective analysis and initialization for the primitive forecast equations. Mon. Wea. Rev., 97, 652-658.
- Panofsky, H. A., and G. W. Brier, 1968: Some Applications of Statistics to Meteorology. The Pennsylvania State University Press, University Park, Penn. p. 200.
- Rodgers, E., R. C. Gentry, W. Shenk, and V. Oliver, 1979: The benefits of using satellite short-interval satellite images to derive winds for tropical cyclones. Mon. Wea. Rev., 107, 575-584.
- Sasaki, Y., 1969: Proposed inclusion of time variation terms, observational and theoretical, in numerical variational objective analysis. J. Meteor. Soc. Japan, 47, 115 - 124.
- Sheets, R. C., 1969: Some mean hurricane soundings. J. Appl. Meteor., 8, 134 - 146.
- Tarbell, T. C., 1979: The initialization of the divergent component of the horizontal wind in mesoscale numerical weather prediction models and its effects on initial precipitation rates. Ph.D. Dissertation. Dept. of Meteorology. Pennsylvania State University. 216 pp.
- Washington, W., 1964: A note on the adjustment towards geostrophic equilibrium in a simple fluid system. Tellus, 16, 530 - 534.

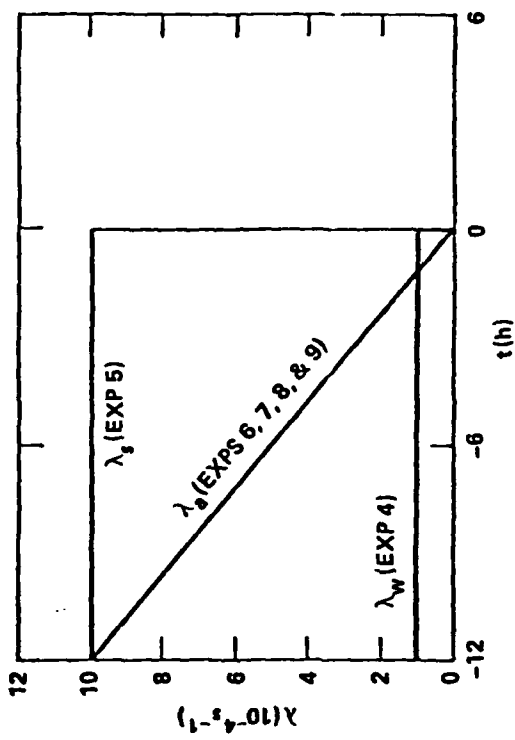
- Williamson, D., and A. Kasahara, 1971: Adaptation of meteorological variables forced by updating. J. Atmos. Sci., 28, 1313-1324.
- Yamada, T: 1976: On the similarity functions A, B, and C of the planetary boundary layer. J. Atmos. Sci., 33, 781 - 793.
- Yu, T.-W., 1980: A marine boundary layer wind analysis scheme for atmospheric circulation models. Third Conference on Ocean-Atmosphere Interaction of the AMS. Jan. 30 - Feb. 1, 1980, Los Angeles, CA.
- Williamson, D., 1973: The effect of forecast error accumulation on four-dimensional data assimilation. J. Atmos. Sci., 30, 537-543.

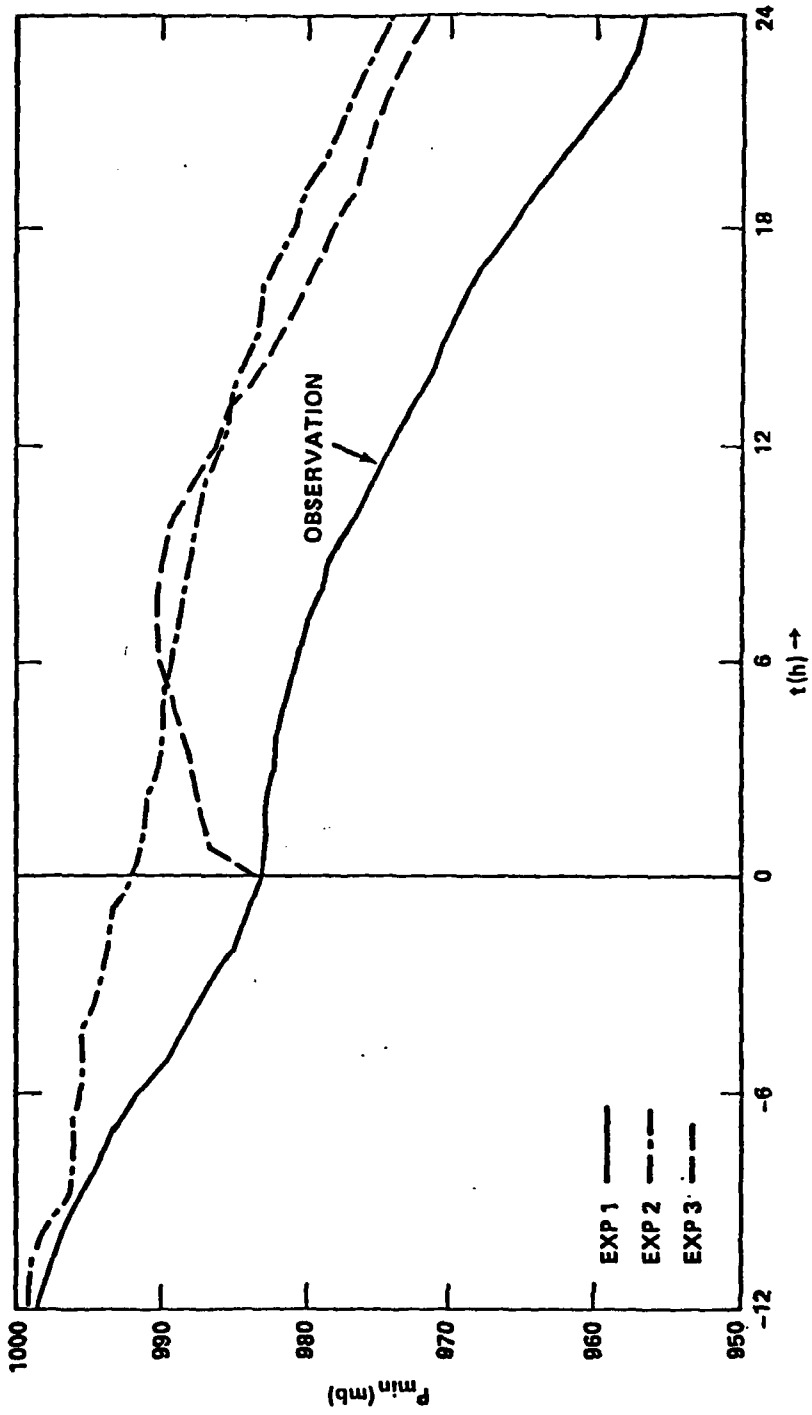
LIST OF FIGURES

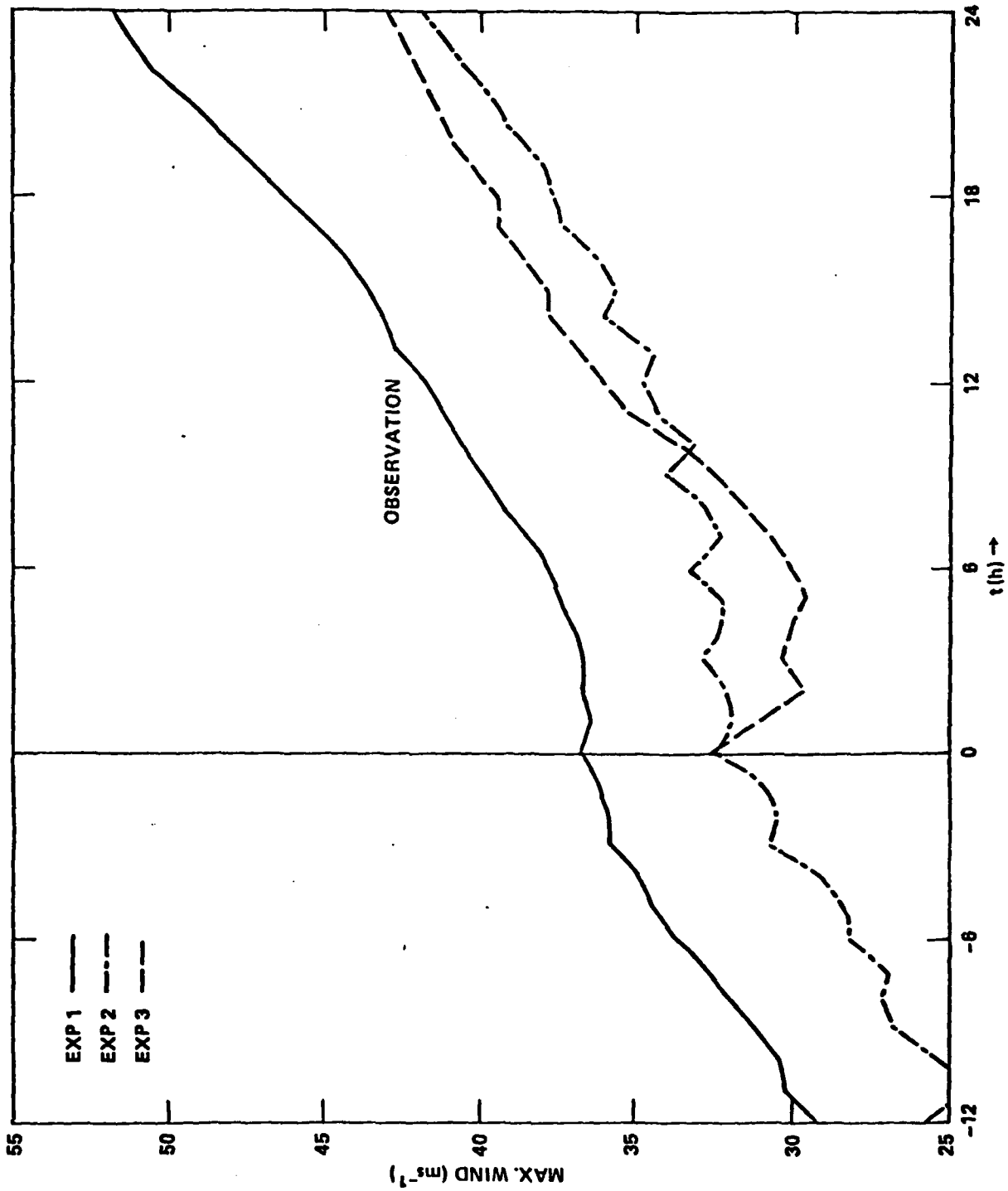
1. Wind speed errors ($m s^{-1}$) in the initial ϕ condition at -12 h after a non-divergent, static initialization.
2. The three relaxation coefficients used in DIR: λ_w for weak relaxation, λ_s for strong relaxation, and λ_a for attenuating relaxation.
3. The minimum pressures of the observation (Exp. 1) and standard forecasts (Exps. 2 and 3).
4. The maximum wind speeds of the observation (Exp. 1) and standard forecasts (Exp. 2 and 3).
5. The time series of the forecast rms errors in total winds for Exps. 2 and 3.
6. The time series of the forecast rms errors in temperatures for Exps. 2 and 3.
7. The time series of the forecast rms errors in specific humidity for Exps. 2 and 3.
8. Same as Figure 3, except for Exps. 4, 5, and 6.
9. Same as Figure 4, except for Exps. 4, 5, and 6.
10. Same as Figure 5, except for Exps. 4, 5, and 6.
11. Same as Figure 3, except for Exps. 7, 8, and 9.
12. Same as Figure 4, except for Exps. 7, 8, and 9.

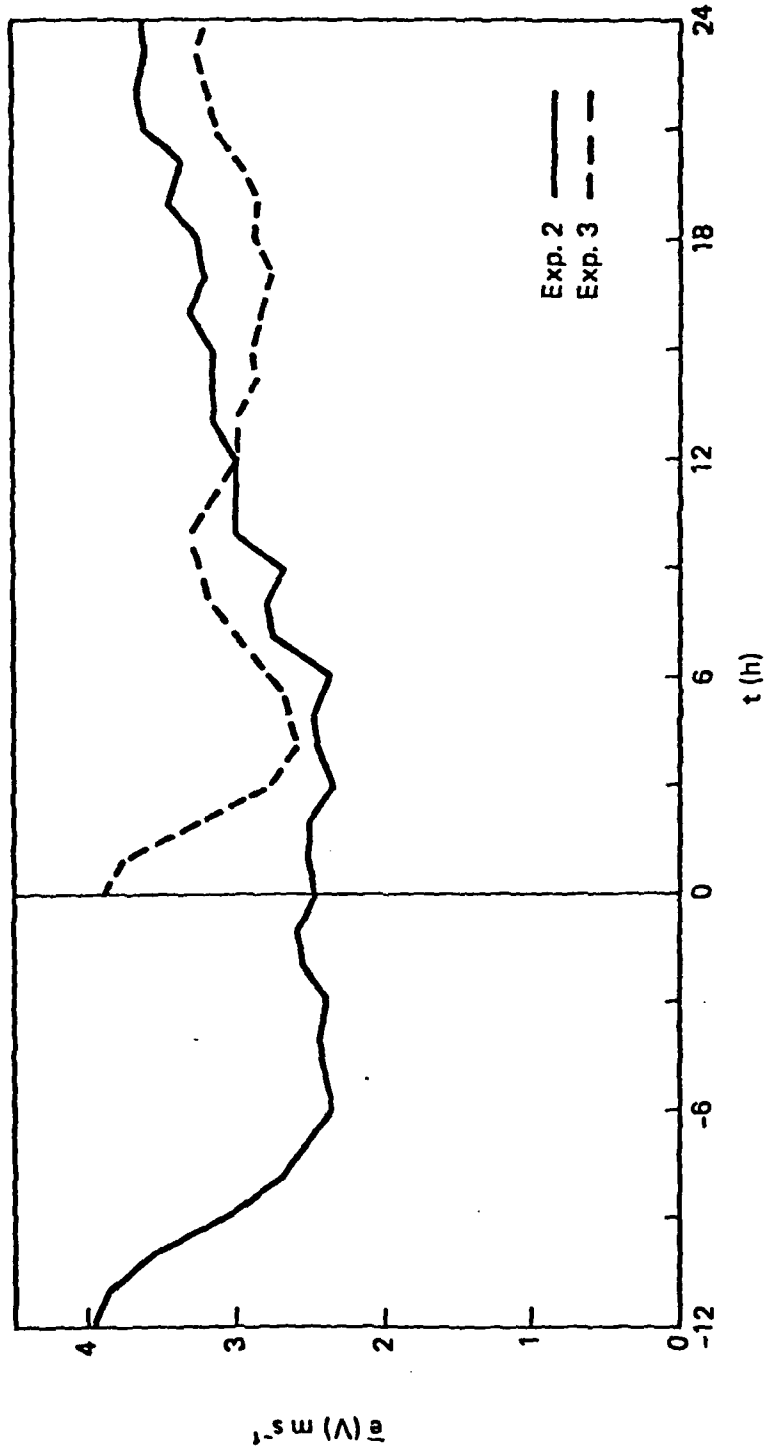
13. The vertical profile of tangential velocity (v) showing the strong vertical shear, and the temperature anomalies (ΔT) showing the warm core at $r = 30$ km at 0 h of the observation.
14. Same as Figure 5, except for Exps. 7, 8, and 9.
15. Same as Figure 6, except for Exps. 7, 8, and 9.
16. Same as Figure 7, except for Exps. 7, 8, and 9.

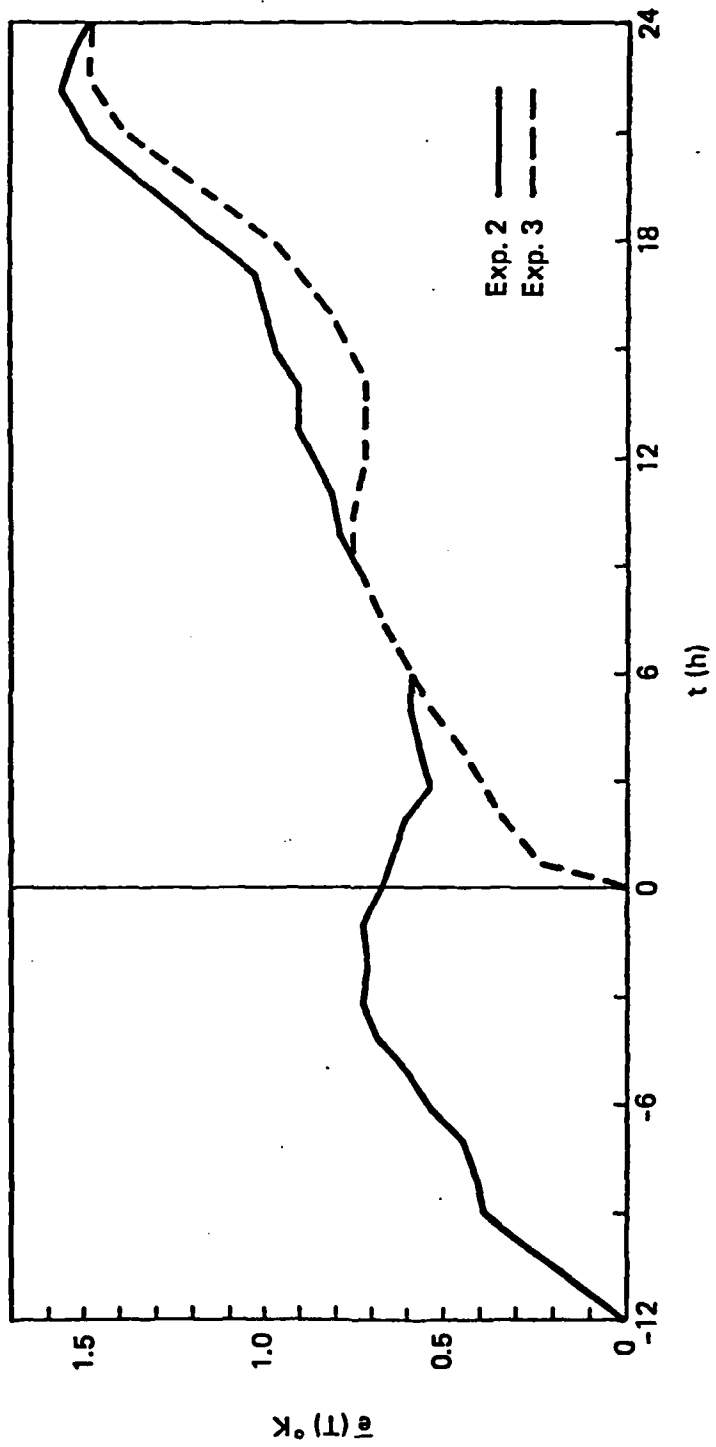


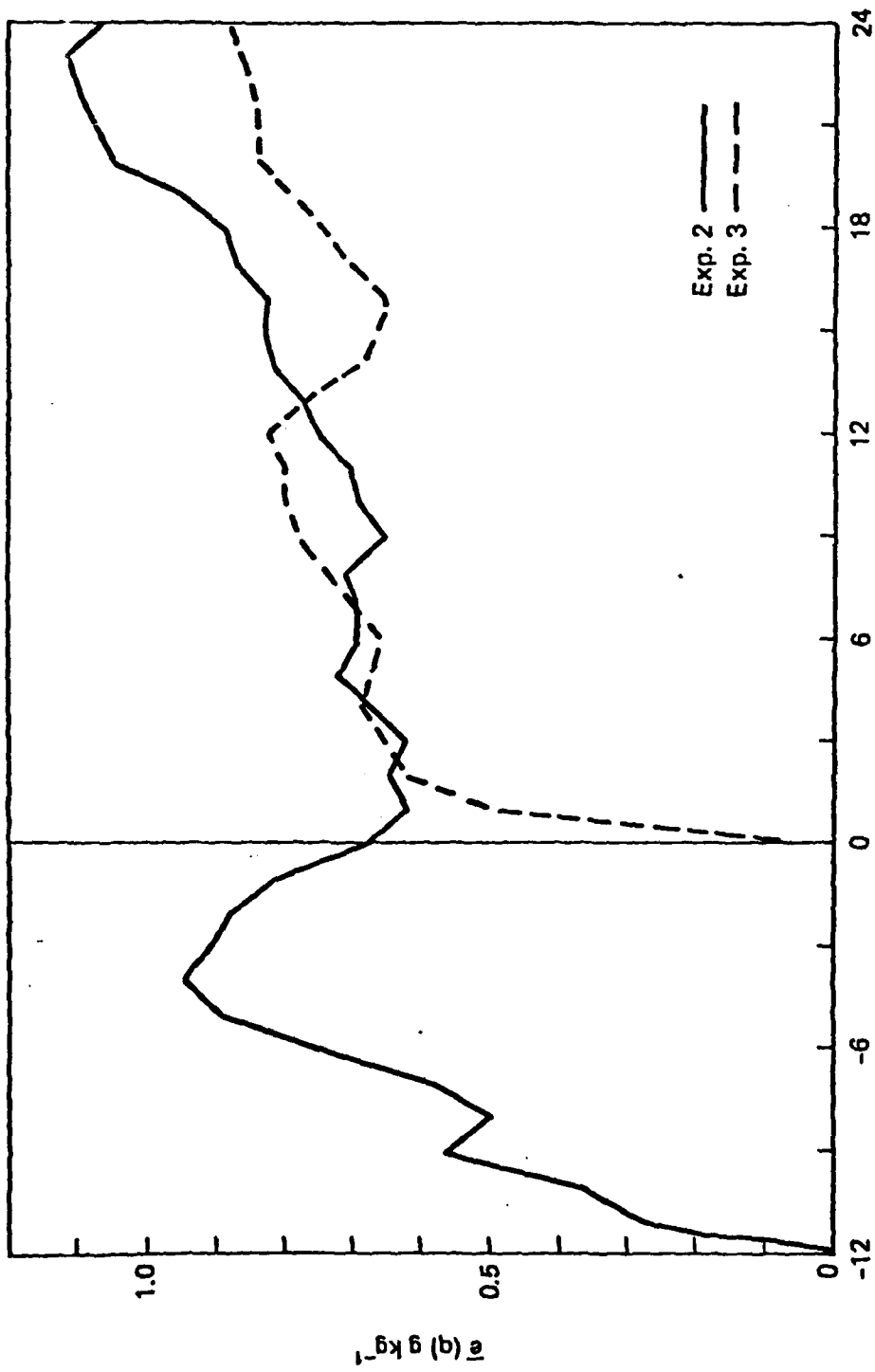




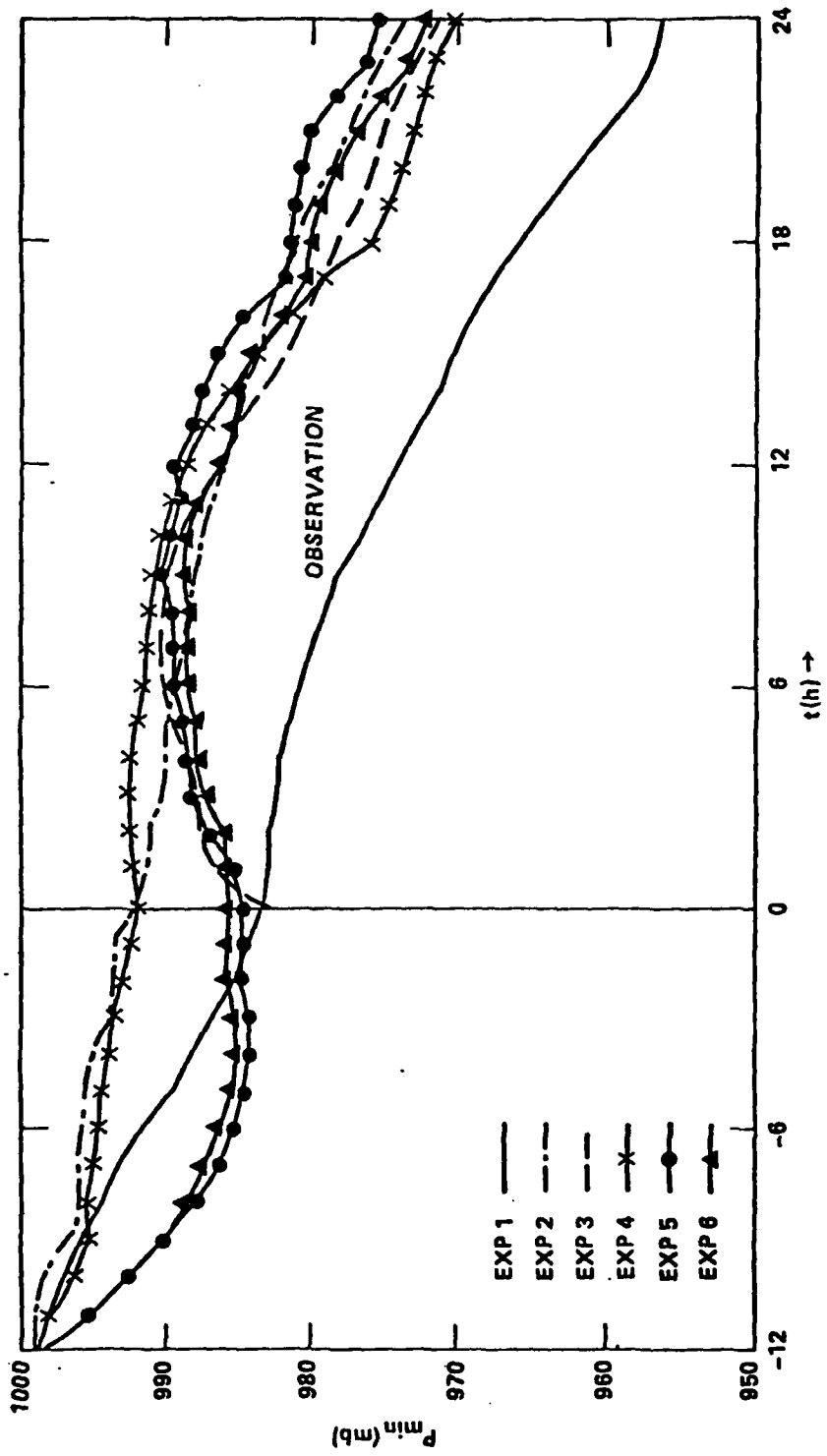


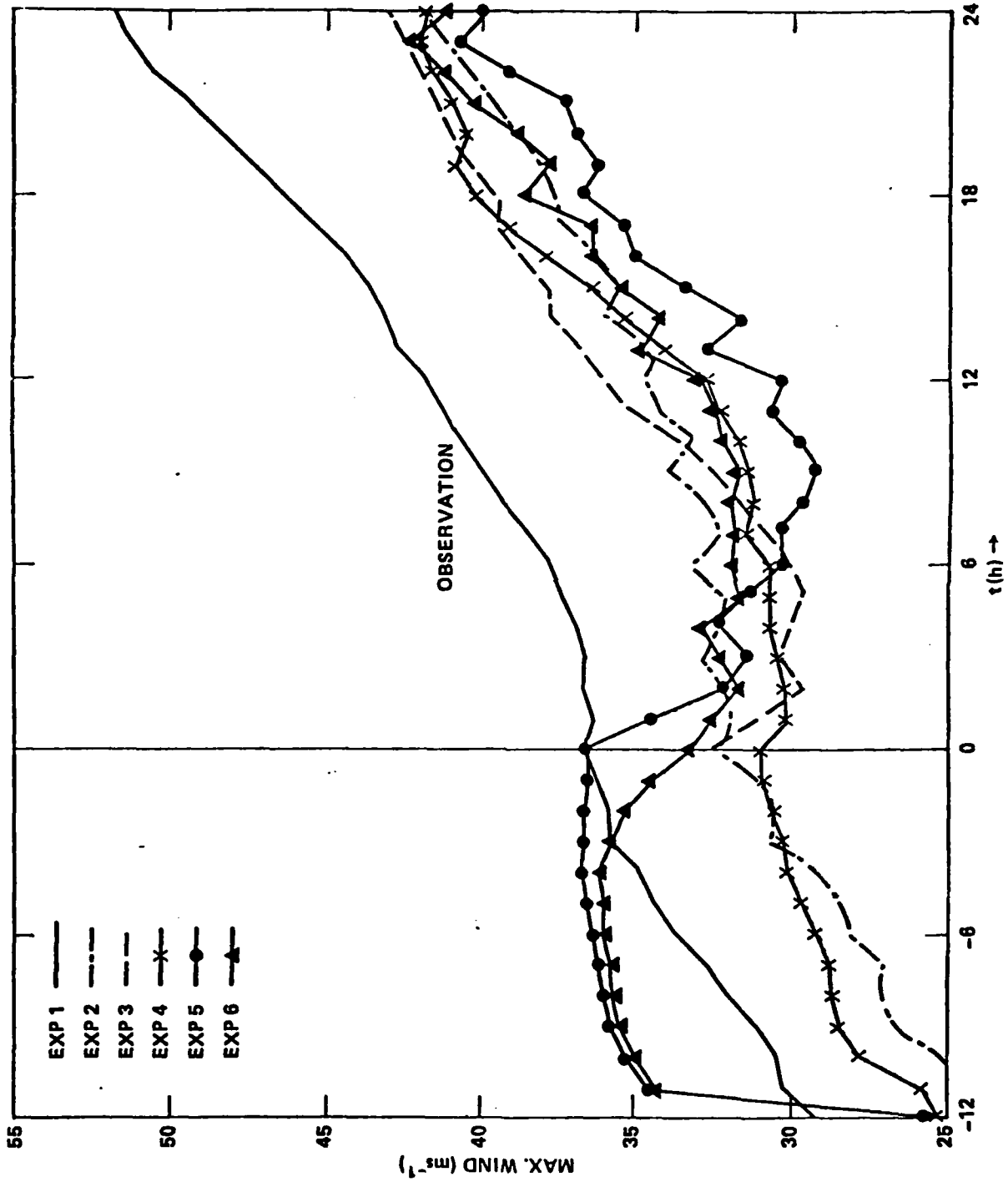


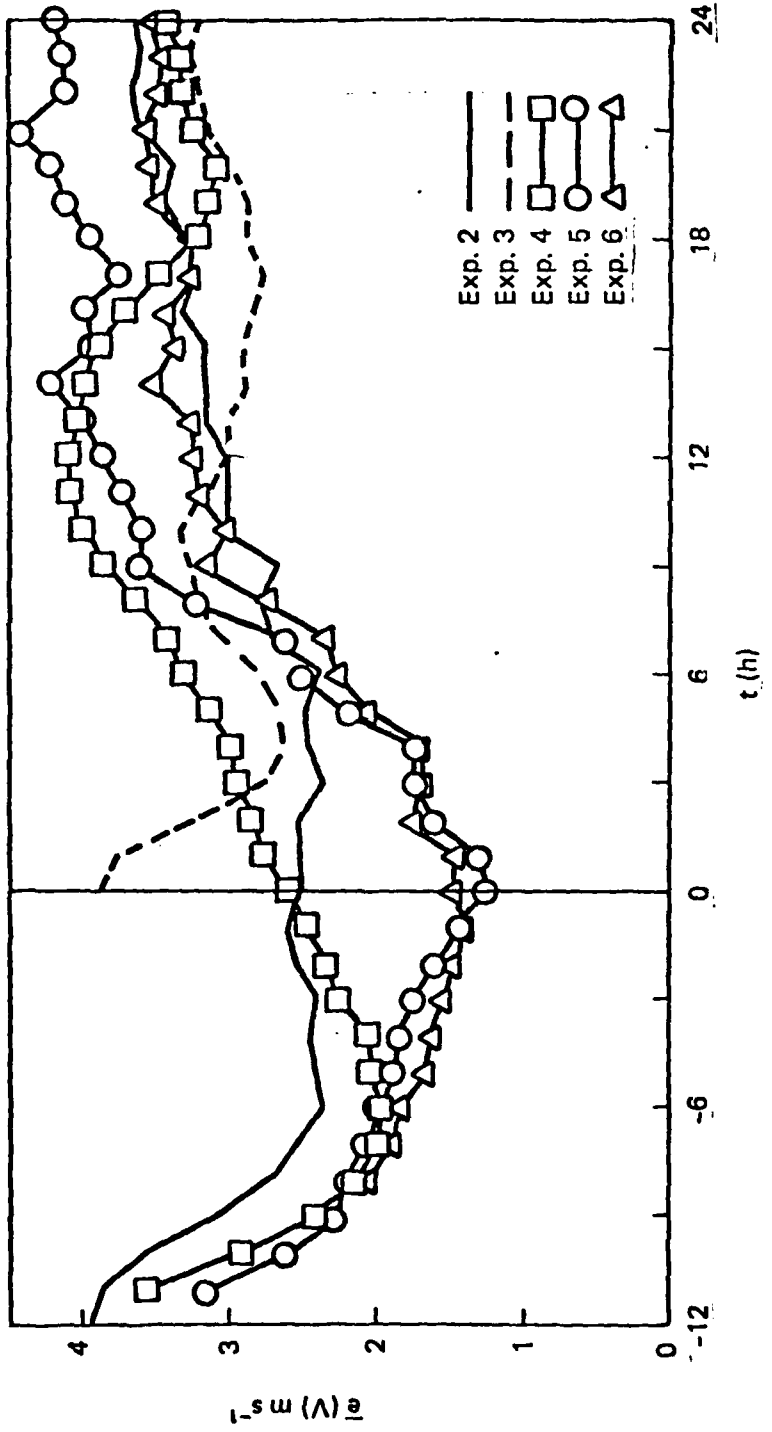


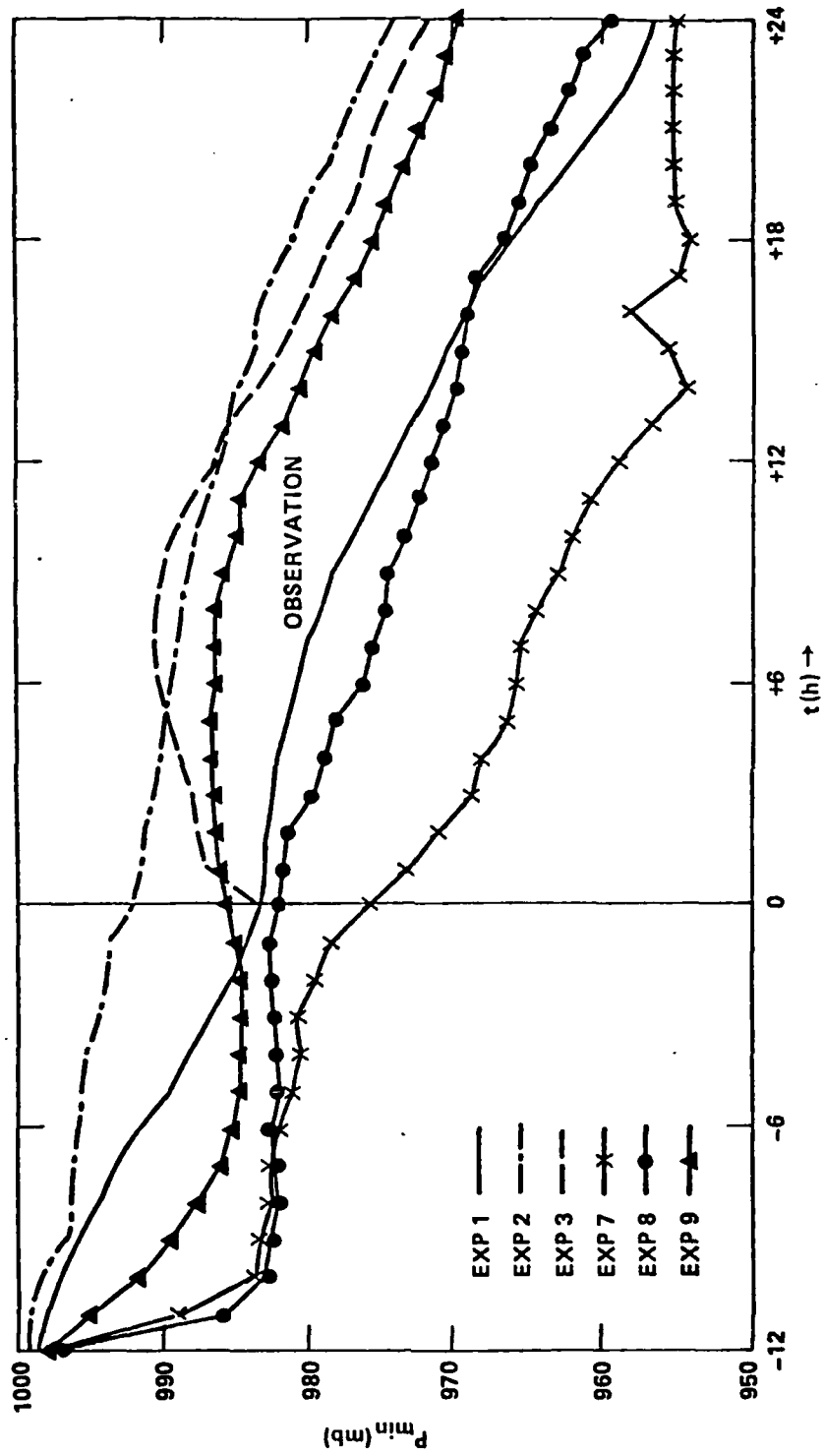


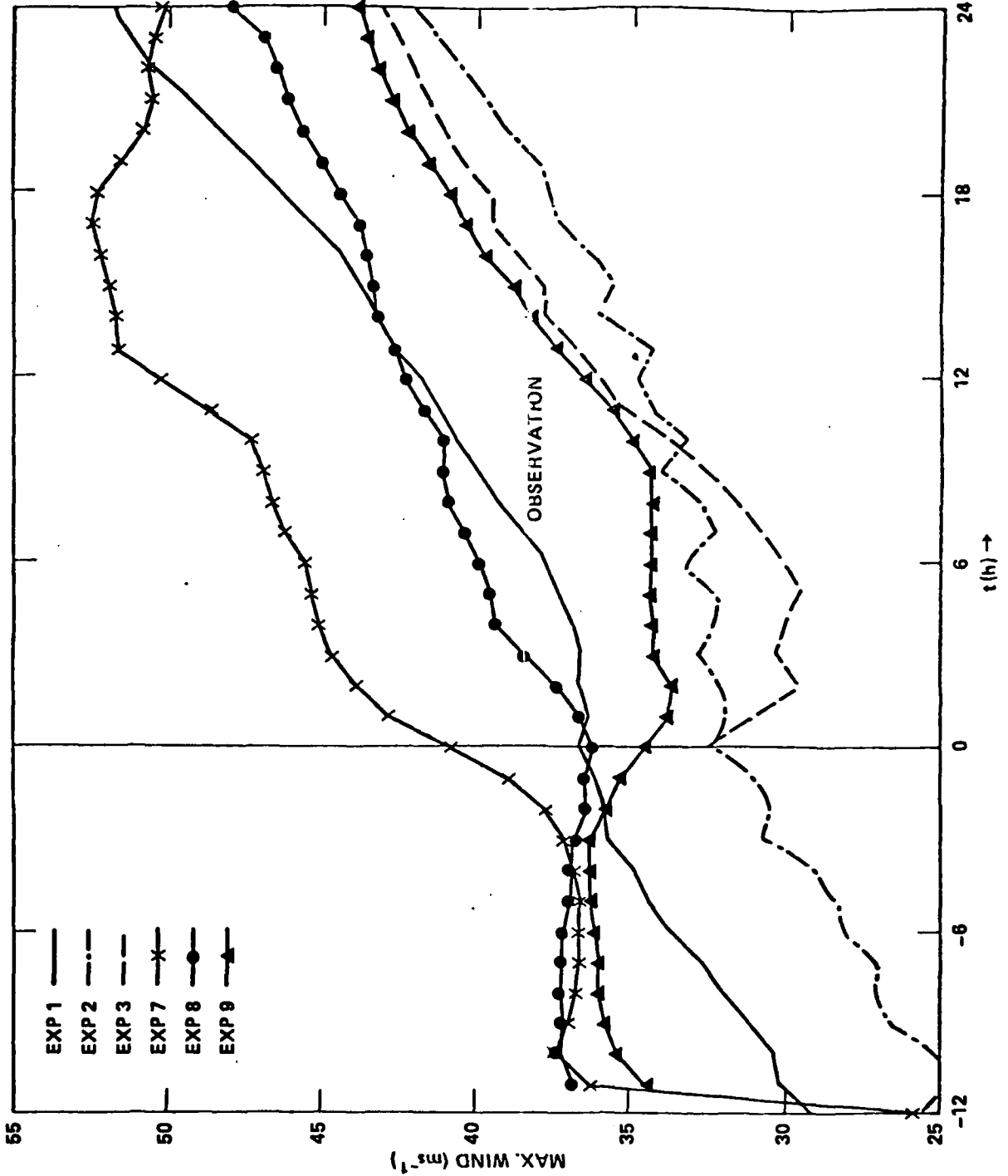
t (h)

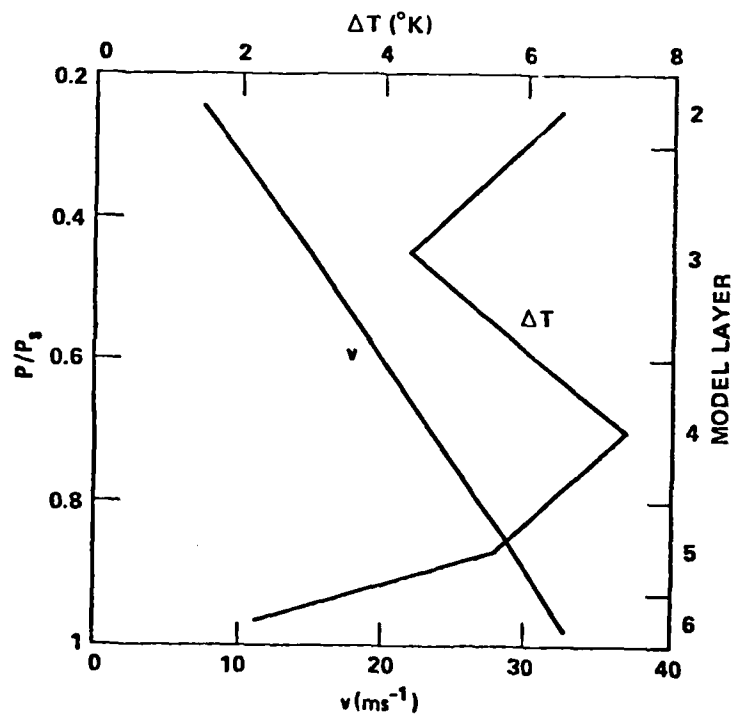


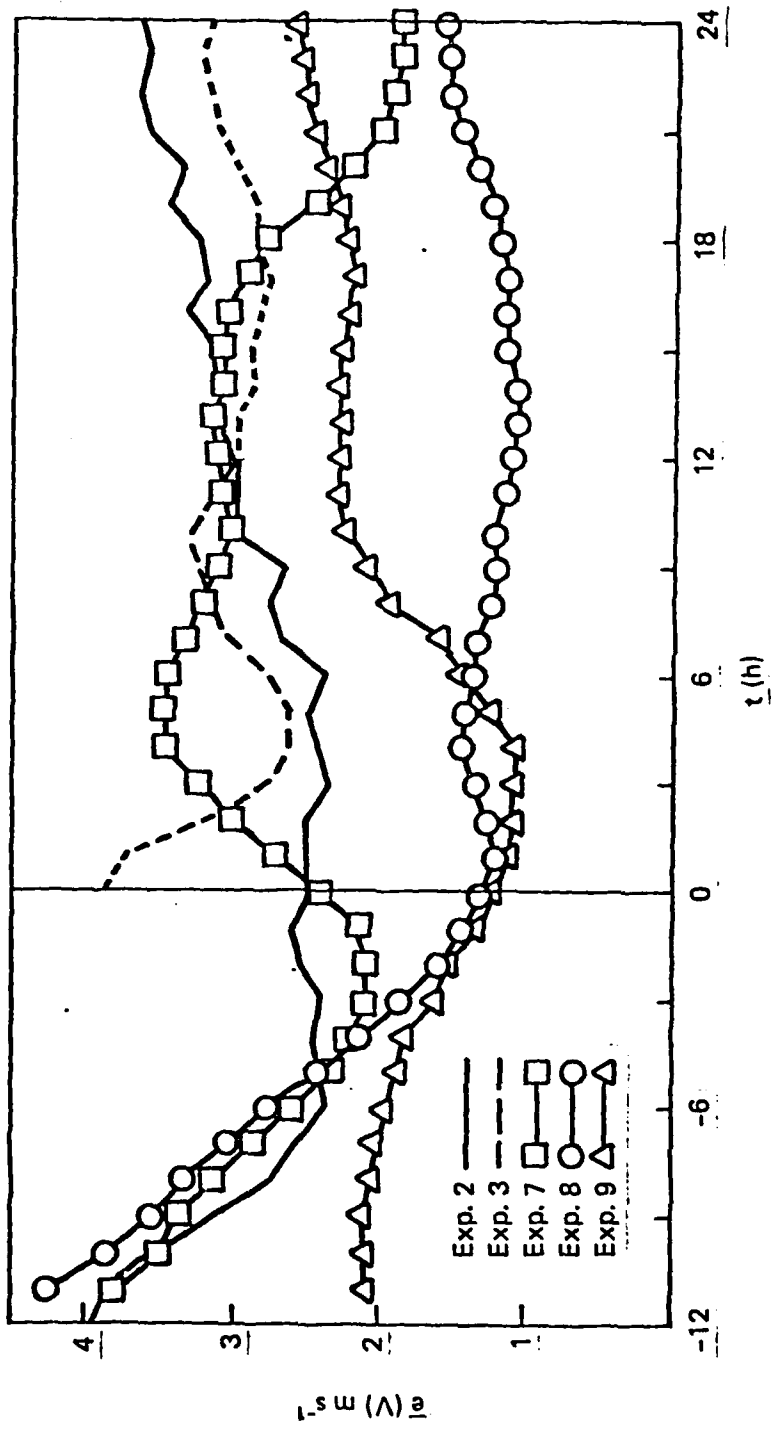


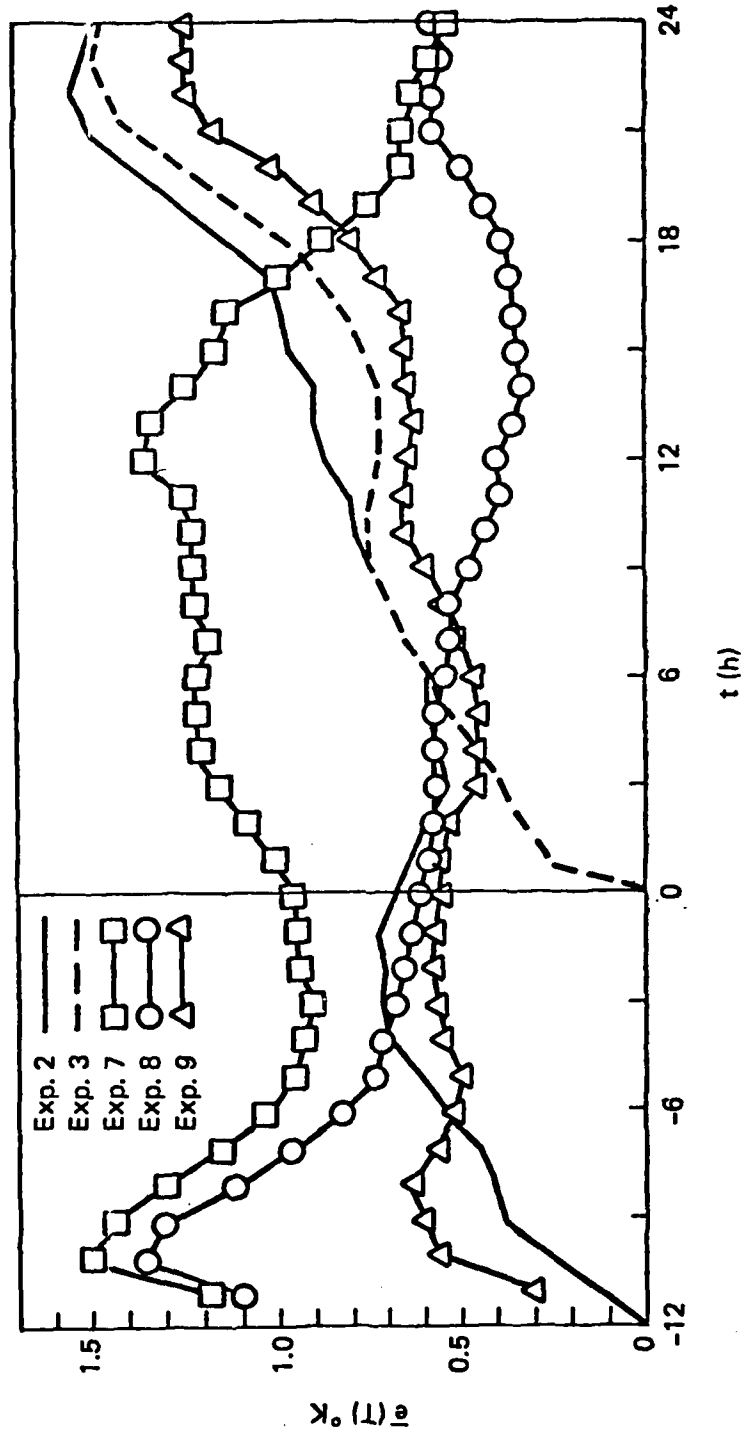


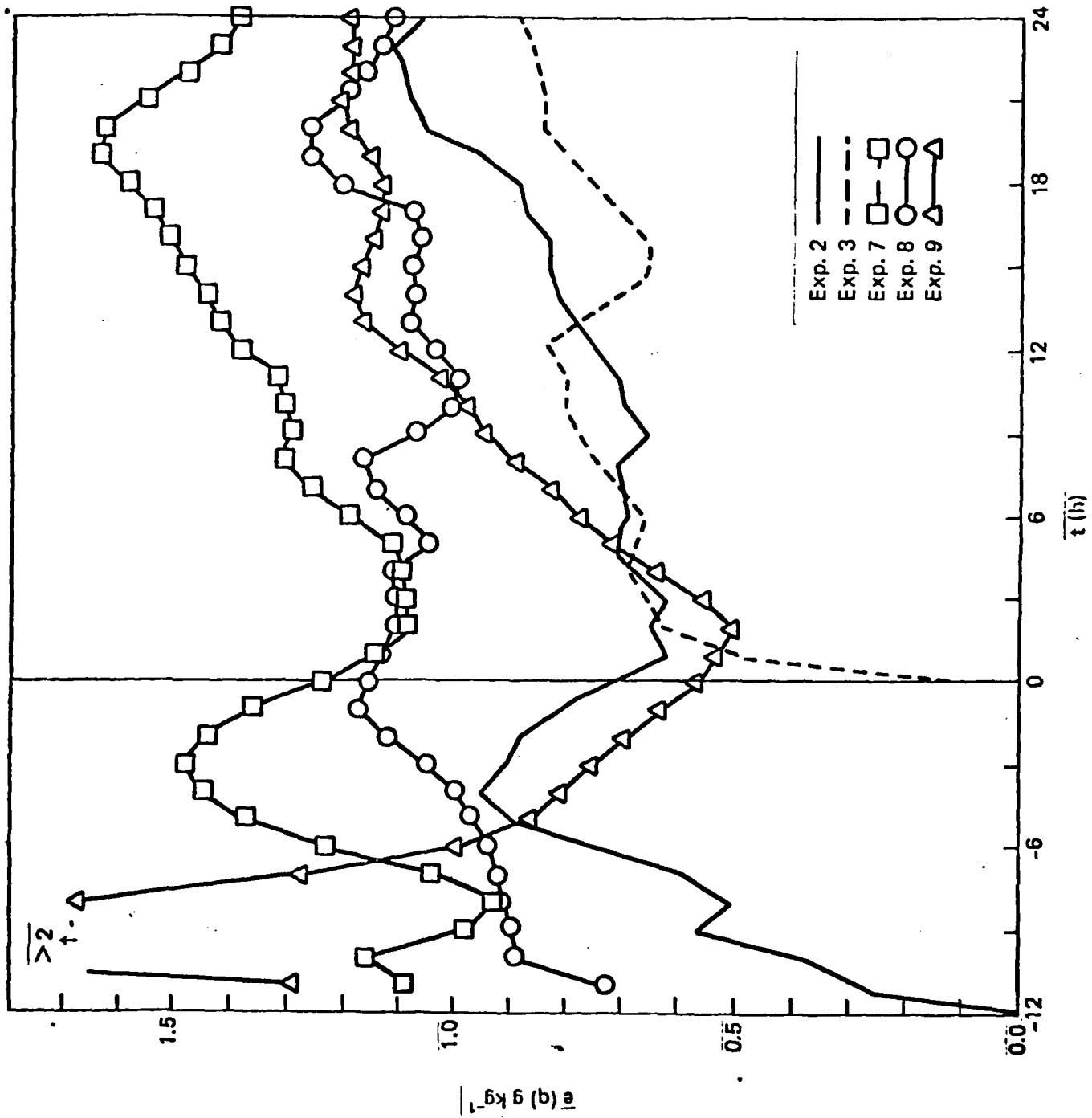












APPENDIX B

NUMERICAL SIMULATION OF THE INFLUENCE
OF SEA-SURFACE TEMPERATURE ON TRANSLATING TROPICAL CYCLONES

Vol. 37 (12), December 1980

ARL Memo Rpt. 4272 July 12, 1980

NUMERICAL SIMULATION OF THE INFLUENCE
OF SEA-SURFACE TEMPERATURE ON TRANSLATING TROPICAL CYCLONES

Simon W. Chang

JAYCOR
205 S. Whiting Street
Alexandria, VA 22304

Rangarao V. Madala

Naval Research Laboratory
Washington, D. C. 20375

August 1980

ABSTRACT

A three-dimensional numerical model with a domain of 3000 x 3000 km and horizontal resolution of 60 km is used to study the influence of sea-surface temperature (SST) on the behavior of tropical cyclones translating with mean flows in the Northern Hemisphere.

We find that tropical cyclones tend to move into regions of warmer SST when a gradient of SST is perpendicular to the mean ambient flow vector (MAFV). The model results also indicated that a region of warmer SST situated to the right side of the MAFV is more favorable for storm intensification than to the left side due to the asymmetries in air-sea energy exchanges associated with translating tropical cyclones. The model tropical cyclone intensifies and has greater rightward deflection in its path relative to the MAFV when translating into the region of warmer SST. The model tropical cyclone intensifies when its center travels along a warm strip, it weakens along, but does not move away from a cool strip.

The results suggest that the SST distribution not only affects the intensity and path of tropical cyclones frictionally, but also affects them thermally. The enhanced evaporation and convergence over the warm SST provide a favorable condition for the growth of the tropical cyclone, and lead to a gradual shift of the storm center toward the warm ocean.

I. INTRODUCTION

Unlike their counterparts in mid- and higher-latitude, where the contrast of air masses provides enough energy for circulation, tropical cyclones depend on the ocean for their energy source. Sensible and latent heat transported through the air-sea interface, in cooperation with the frictionally-induced inflow, supplies the energy for maintaining the tropical cyclone circulation. The air-sea interaction is an important physical process that affects the behavior of tropical cyclones.

Observational studies on the interaction of tropical cyclones and the ocean have indicated a strong dependence of tropical cyclones on the sea-surface temperature (SST). The development, intensification, and movement of tropical cyclones are in many instances linked with the warm SST (Palmen, 1948; Fisher, 1958; Miller, 1958; Perlroth, 1967; Brand, 1971; Gray, 1979). Because the ocean is regarded as the heat reservoir, attention has also been focussed on the importance of the thermal structure of the upper ocean. It is found that warm and deep oceanic mixed layers are necessary conditions for the development and intensification of tropical cyclones (Tisdale and Clapp, 1963; Perlroth, 1969). Contrary to the above findings, some tropical cyclones are not affected by SST (Ramage, 1972; 1974). Because many other factors can influence the behavior of tropical cyclones, it is very difficult to isolate the effects of SST from observational data.

Earlier numerical studies with axisymmetrical (therefore stationary) models showed that tropical cyclones are very sensitive to small changes of SST (Ooyama, 1969, Rosenthal, 1971; Sundquist, 1972). Typically, a 50% change in model maximum wind would result from a 2°C change of SST. By incorporating a more sophisticated parameterization of the atmospheric boundary layer (ABL),

Anthes and Chang (1978) showed that an axisymmetric tropical cyclone is not as sensitive as earlier studies indicated. The enhanced (decreased) evaporation associated with warm (cool) SST is partially compensated for by the increased (decreased) surface friction, therefore, the tropical cyclone has a 12h delay in response to SST changes. When their tropical cyclone was coupled with the ocean, the response was even weaker and further delayed (Chang and Anthes, 1979). However, the long term behavior of their model cyclone still agreed with previous axisymmetric model studies, i.e., warmer SST results in intensification and cooler SST results in weakening.

The motion of a tropical cyclone with mean flow over an ocean of uniform SST has been studied by Kuo (1969) and Jones (1977a) using linear models. The air-sea interactions in these two linear models were purely mechanical with only surface friction. These studies indicated that the trajectory of the vortex center is a damped trochoid. The deflection angle of the mean path (the angle between the mean current and the mean vortex motion) is a function of the surface friction and the environmental friction. For tropical cyclones, where the surface friction is greater than the environmental friction, the deflection is usually to the right of the mean flow. These results were later substantiated by Jones' (1977) three-dimensional, non-linear model with uniform SST.

The behavior of tropical cyclone in a three-dimensional model with mean flow over non-uniform SST has not been studied. With variations in SST, both the intensity and movement of tropical cyclones may be more complex. The surface friction will change because of variations in surface stability associated with the non-uniform SST, the sensible and latent heat exchanges may be in certain ways dictated by the SST distributions. These variations may significantly affect the behavior of tropical cyclones.

The purpose of this study is to investigate the influence of various non-uniform SST distributions on the intensities and movements of tropical cyclones that are imbedded in a mean flow. As described in the next section, the model domain is large enough to allow free movement of the tropical cyclone for about 3-4 days. The parameterization of the ABL has been improved so that the air-sea interaction is adequately treated. In Section III, the life history of a weak tropical cyclone translating over ocean with uniform SST will be discussed and used as the control experiment for later comparison. In Section IV, we first examine the responses of tropical cyclones when translating into regions of warmer and cooler SST. In Section V, the response of the translating tropical cyclone with SST gradients perpendicular to the mean flow will be discussed. Finally, the response of the translating tropical cyclone encountering strips of warmer or cooler SST will be discussed in Section VI.

II. THE NUMERICAL MODEL

The tropical cyclone model used is identical to the one described in Madala and Chang (1979)⁽¹⁾. The governing equations include the primitive equations of conservation for horizontal momentum, mass, enthalpy, and water vapor. The system of equations is hydrostatic. A normalized pressure (σ) is the vertical coordinate (Phillips, 1957). The physics includes the subgrid scale horizontal mixing, the subgrid scale cumulus convection, the grid scale precipitation, and the subgrid scale vertical mixing due to surface friction.

The subgrid scale horizontal mixing is parameterized by a kinematic eddy coefficient. This coefficient consists of a constant part and a part linearly

dependent on wind speed. This form of the eddy coefficient yields suitable mixing in the initial as well as the mature stages (Anthes et al. 1971).

The subgrid scale cumulus convection is parameterized following Kuo's (1974) and Anthes's (1977) methods. Conditional instability and the boundary layer convergence of water vapor are prerequisites for the cumulus convection. The partitioning of heating and moistening depends on the vertically averaged relative humidity of the air column. The vertical distribution of heating is determined by the amount of conditional instability and the prescribed weighting functions (see Anthes and Chang, 1979). The use of the weighting functions insures a proper vertical heating distribution for the growth of tropical cyclone scale disturbances. The grid scale precipitation occurs when the air reaches saturation in grid scale lifting.

The boundary layer effects are parameterized based on a generalized similarity theory in which the logarithmic-linear profiles of the momentum, temperature, and water vapor are "match" into the mixed layer (Chang and Madala, 1980).⁽²⁾ Anthes and Chang (1978) have shown a higher resolution BL is superior to a single layer bulk ABL in an axisymmetric tropical cyclone model. To incorporate into a 3D tropical cyclone model a higher resolution ABL is economically prohibitive. In addition, the results of Anthes and Chang (1979) indicate that, except for the period of rapidly changing stability, the ABL in tropical cyclones with strong winds and small Richardson numbers is dominated by mechanical mixing and is nearly invariate in height. Therefore, matching technique with fixed ABL height seems to be appropriate. Universal functions A, B, C, and D are formulated following Yamada (1976). The surface roughness height over open water are calculated by Charnock's equation (Delsol et al., 1970).

The model atmosphere from $P = P_s$ (surface) to $P = 0$ is divided into seven sigma layers (Figure 1). Note that the lowest layer has a thickness of about 700 m, which is the typical BL depth in tropical cyclones (Moss and Merceret, 1976; Anthes and Chang, 1978; Chang and Anthes, 1979). A better vertical resolution between $\sigma = 0.1$ and $\sigma = 0.3$ is used to resolve the tropopause and outflow structure. All prognostic variables such as u and q , are defined at the center of each layer, all diagnostic variables such as $\dot{\sigma}$ and ω are defined at the boundary of each layer. The momentum points and mass points are fully staggered in horizontal direction following the scheme C in Arakawa and Lamb (1977). The uniform horizontal resolution is 60 km throughout the model domain of 3000 x 3000 km. We take note that a horizontal resolution of 60 km is marginal in resolving the detail structure near the storm center. However, a resolution of 60 km is a reasonable compromise for the time and space scales of this study. The spatial differencing is second order to conserve mass, momentum, and enthalpy. The newly developed split-explicit method is applied for temporal integration. The boundary conditions are Neuman for all dependent variables. A sponge boundary condition is applied to the momentum to control noise at lateral boundaries.

The tropical atmosphere of the hurricane season (Sheets, 1971) is used for the initial mean thermodynamic state of the model. The thermal structure features a conditionally unstable lapse rate from surface to about 350 mb and high relative humidity (RH) up to 500 mb.

The initial flow field includes a uniform easterly current of about 4.5 m s^{-1} and a non-divergent, idealized vortex with maximum wind of 16 m s^{-1} . The initial surface pressure and temperature field are in gradient balance with the flow field. The Coriolis parameter is $5 \times 10^{-5} \text{ s}^{-1}$. One effect

of latitudinal variation of Coriolis parameter is to produce a northward movement of the vortex (Madala and Piacsek, 1975; Anthes and Hoke, 1975). For the purpose of isolating the movement of tropical cyclones caused by SST, the Coriolis parameter is set constant in this study.

III. THE CONTROL EXPERIMENT

A tropical cyclone with rather weak intensity develops from the initial vortex imbedded in the uniform easterly mean flow of approximately 4.5 m s^{-1} over an ocean of 28.5 C . The model tropical cyclone reaches a quasi-steady state after 48 h, attaining a minimum pressure of 996 mb^{-1} and maximum ABL wind speed in the lowest layer of the model of 32 m s^{-1} (this experiment is referred to as the control experiment (Exp. A, see Table 1)).

Figure 2 shows the ABL flow pattern and the surface pressure field at 84 h when the model integration was terminated. The strong circulation is confined to the region near the storm center. Maximum winds are located to the right of the storm track where the cyclonic circulation and the mean current is in the same direction. The winds at the center are very weak. The flow far from the storm circulation is nearly undisturbed by the storm. These characteristics of the low-level flow are also implied by the surface pressure field. The circular isobars and the stronger pressure gradient are concentrated to the region near the storm center.

Contrary to the concentrated cyclonic circulation at low level, the asymmetric flow at the outflow level ($\sigma = 0.1 - 0.2$) is predominantly anti-cyclonic with a small region of cyclonic circulation near the center. The speed of the anticyclonic circulation increases away from the center in conservation of the angular momentum. It reaches a maximum of more than 20 m s^{-1} to the southeast* of the storm center.

* Because the Coriolis parameter is constant, the orientation of the domain has no real geophysical meaning.

As shown by the paths of the storm center (defined by the surface pressure field), the storm moves downstream with the mean current and with a deflection to the right of the MAFV. At 84 h, the net northward displacement of the storm center is about 100 km. The 5° deflection angle of our model is very typical for model tropical cyclones (Jones, 1977a). However, the small scale looping motion in the trochoid (Jones, 1977b) cannot be resolved by the 60 km grid resolution of the present model.

Figure 3 shows the stress field at 84 h of Exp. A. Comparing with the surface wind field, the region of the strongest stress is located to the right of the storm track. The crescent shape of the maximum stress region is responsible for the often observed crescent-shaped maximum cooling in the ocean (Black, 1972). To the south of the strong stress, there is a region where the stress is very small, corresponding to the weak surface wind at the storm center.

The evaporation rate at 84 h of Exp. A shows that the strongest evaporation occurs outside and to the north of the region of the maximum wind (Fig. 4) where the ABL winds are considerable and the humidity is undersaturated. The maximum evaporation rate is approximately 2.5 cm day^{-1} . The sensible heating is relatively insignificant, in agreement with earlier findings of Rosenthal (1971) and Anthes and Chang (1978).

A series of experiments with various non-uniform SST distributions were performed. The schematical patterns of SST tested are shown in Figures 5 and listed in Table 1.

IV. TROPICAL CYCLONES TRANSLATING INTO BROAD REGIONS OF WARM AND COOL SST

As mentioned before, the intensity of axisymmetric, stationary model tropical cyclones is sensitive to sudden changes of SST. The situation that

Table 1. SUMMARY OF EXPERIMENTS AND RESULTS

Experiment	SST Patterns	Path	Final Max. Wind (m s ⁻¹)
A	Uniform SST, 28.5 C	~5° to the right of MAFV	33
W	Broad region of 2 C warmer SST	~7° to the right of MAFV	50
C	Broad region of 2 C cooler SST	~3° to the right of MAFV	22
WR	Warmer SST to the right with gradient perpendicular to MAFV	Moves toward warm SST deflection angle ~17°	50
WL	Warmer SST to the left with gradient perpendicular to MAFV	Moves toward warm SST deflection angle ~-5°	31
WS	2 C warm strip parallel to MAFV	Same as Control	50
CS	2 C cool strip parallel to MAFV	Same as Control	25
WS45	2 C warm strip at 45° angle to MAFV	Same as Control	34

we consider here is a tropical cyclone that translates into regions of warmer or cooler SST. The response of the tropical cyclone in this more realistic situation is investigated with Exp. W., where the SST is 2 C warmer at 30.5 C in the western half of the domain, and Exp. C, where the SST is 2 C cooler at 26.5 C in the western half of the domain. SST in the eastern half of the domain stays at 28.5 C.

Figure 6 shows the time series of the minimum pressures of Exps. W and C and the control (Exp. A). In both Exps. W and C, the minimum pressures deviate very little from the control experiment until the center of the storm moves into the region of warmer or cooler SST. The delay is also evident in the maximum surface wind which does not deviate significantly from the control until after 36 h (Figure 7). This delayed response, similar to the behavior of the axisymmetric model of Anthes and Chang (1978), is due to the increased (decreased) dissipation of kinetic energy which partially compensates for the enhanced (weakened) evaporation over the warm (cool) SST.

The SST patterns tested here also affect the path of the tropical cyclone. At 84 h, the storm centers in Exps. W and C are displaced to about 60-100 km to the right and left, respectively, relative to the control experiment (Figure 8). The fact that the increased surface friction produces a stronger deflection to the right of the MAFV agrees qualitatively with the linear models of Kuo's (1969) and Jones' (1977a). But in contrast to the linear theory, the variation in the surface friction may be due to both storm intensity and the surface stability. As it becomes clearer in the experiments discussed in the next section, the asymmetries associated with a translating tropical cyclone and air-sea thermal exchange can also contribute to the deflection. Most of the air-sea exchanges of sensible and latent heats occur in the right half of

the tropical cyclone relative to the MAFV, and have important thermal effects on the paths of tropical cyclones other than the mechanical effects considered previously. As shown in Figure 9, stronger evaporation mainly occurs over the region of warmer SST at 27 h of Exp. W. The maximum evaporation rate increases from about 2 cm day^{-1} at 24 h to more than 6 cm day^{-1} at 36 h in Exp. W when the center of the storm moves into the region of warmer SST. Such a strong and asymmetric evaporation distribution causes a stronger convection and heating to the right of the MAFV and shifts the storm center toward the north.

V. TROPICAL CYCLONE TRANSLATING PERPENDICULAR TO SST GRADIENT

To further differentiate ocean's thermal effect on the path of tropical cyclones, we now consider the case that the mean flow is perpendicular to SST gradient. In Exp. WR, the SST is 30.5 C to the right and 26.5 C to the left of the MAFV, and in between the 30.5 C and 26.5 C waters, there is a 600-km wide region where the SST increases continuously toward the right having a gradient of $4 \text{ C}/600 \text{ km}$. In Exp. WL, the SST pattern is reversed so that the warm and cool ocean waters are located to the left and right of the MAFV, respectively, and the SST gradient is toward the left in the central region.

These SST patterns have very noticeable influence on both the intensity and the path of the model tropical cyclone. As illustrated in Figs. 10 and 11, the storm intensity of Exp. WR increases greatly to a central pressure of 982 mb and maximum wind of 50 m s^{-1} at 84 h; whereas the storm intensity in Exp. WL remains essentially unchanged. The storm centers

in both Exps. WR and WL are displaced perpendicular to the MAFV from the control experiment by more than 200 km toward the regions of warmer SST (Fig. 12). At 84 h, the center of circulation in Exp. WR has almost entered the region of 30.5C water. The apparent tendency of the model tropical cyclone to move toward the warm SST is caused by the enhanced latent heating associated with the SST distributions.

As illustrated by Figures 13 and 14, the evaporation in Exp. WR occurs mainly over the warm water to the right of the MAFV and to the rear of the storm where the air flows into warmer water. The strong evaporation in Exp. WL is obviously biased toward the southwest of the storm center. Both the rate of evaporation and the area of strong evaporation in Exp. WR are much larger than in Exp. WL. Due to the asymmetry associated with the translating tropical cyclone, the surface wind and the surface stress are stronger to the right of the MAFV (see Figure 2 and 3). In Exp. WR the region of stronger stress coincides with the region of warmer SST, whereas in Exp. WL, the region of stronger stress does not coincide with the region of warmer SST. Consequently, the maximum evaporation rate increases to 6~7 cm d^{-1} in Exp. WR, it remains at about 2 cm d^{-1} in Exp. WL.

The overall stronger evaporation in Exp. WR causes the storm to intensify. Increased evaporation and enhanced surface friction also cause a local increase in the latent energy convergence over the region of warmer SST. Thus provides a favorable condition for the growth of the tropical cyclone. The stronger convergence and hence the enhanced cumulus heating over the warmer SST cause the center of circulation to shift toward the warm water. The shift is then followed by the pressure field through adjustment process. This can be illustrated by the isobar patterns and flow fields at 48 h (Figures 13 and 14). The flow fields shown are at the level of $\sigma = 0.66$,

which would nearly be in gradient balance with the pressure field under steady state and stationary conditions. It is apparent in Figures 13 and 14 that the circulation centers are ahead of the low pressure center in their movements toward the warmer SST. The isobars are not concentric with weaker pressure gradients located toward the warm SST, indicating the shift of the mass field toward the warmer ocean.

Note also that the rightward deflection from the control path in Exp. WR is larger than that in Exp. W, and the leftward deflection from the control path in Exp. WL is larger than that in Exp. C, where the storm intensity is weaker than Exp. WL. This behavior cannot be explained by the linear theories where the hurricane-ocean interaction is merely mechanical. The SST distribution causes a redistribution of the latent heating, and shifts the circulation center toward the region where the growth of the tropical cyclone is favorite.

Several investigators have used the total thermal potential³ as a measure of the energy available for the development of incipient tropical cyclones (Perlroth, 1969; Leipper and Volgenan, 1972). As illustrated by Exps. WR and WL, the storm intensities and paths are very different in spite of the fact that the total oceanic thermal potentials in two cases are identical. This confirms the finding in Chang (1979) that the air-sea energy exchange in the tropical cyclone and ocean system depends very much on the details of the relative location, size, and magnitude in SST variations.

VI. TROPICAL CYCLONE TRANSLATING INTO STRIPS OF WARM OR COOL SST

We now examine the response of the tropical cyclone when it passes over strips of warmer or cooler SSTs. As depicted in Figure 5, the SST patterns include (1) a 300-km-wide 2C warm strip parallel to the MAFV (Exp. WS), (2) a 300-km-wide 2C cold tongue parallel to the MAFV (Exp. CS), and (3) a 300-km-wide 2C warm strip at 45° angle to the right of the MAFV.

The response of the model tropical cyclone to the warm or cold strip is not noticeable until after 36 h when the center of the storm moves into the warm or cold tongue. At 84 h, the minimum pressures of Exps. WS and CS are respectively 980 and 1000 mb, and the maximum surface winds are respectively 50 and 25 m s^{-1} (Figures 15 and 16).

Contrary to the finding that tropical cyclones tend to steer away from a pool of cold ocean water (e.g., Brand, 1971), the paths of the storm centers in Exps. WS and CS are essentially unchanged as compared to the control Exp. A despite the difference in storm intensity (Figure 13). It is probably due to the fact that the changes in surface friction are restricted to the relatively small regions of warm or cold strips. The gradual shift of the vortex toward the region of warm ocean evident in Exps. WR and WL does not occur in Exp. CS because the warmer water is not immediately adjacent to the center of the storm.

The model tropical cyclone has very little response to the warm strip which lies at 45° angle to the MAFV (Exp. WS45). Previous experiments with axisymmetric hurricane model (Anthes and Chang, 1978; Chang and Anthes, 1979) showed that a tropical cyclone does not respond to warm SST if the

tropical cyclone overlays the region of warmer SST for less than 12 h. The storm in Exp. WS45 travels through the region of warmer SST in less than 15 h, which is apparently not long enough for the tropical cyclone to have significant response before it leaves the warm strip.

The variation in SST affects the air-sea exchange of sensible and latent heat. As shown by Figure 14, the strong evaporation at 30 h of Exp. WS occurs mainly in the region of the warm SST. The strongest evaporation occurs near the leading (northern) edge of the warm tongue. The evaporation in Exp. CS is much weaker over the cold tongue except for a slight increase where the air flow re-enters the region of 28.5C water. Changes in the evaporation near the storm center, over a period of time, results in changes in the intensities of the tropical cyclone. There are many other fine details in the momentum field of the tropical cyclone induced by the warm and cold strips. For example, before the center of the tropical cyclone and the major portion of the strong cyclonic circulation enter the region of change SST, the low-level flow reacts to the warm strip in a fashion similar to that of a heat island. Upward motion is induced in the ABL due to temperature gradient within the edge of the warm ocean. These changes in the momentum field are persistent, but localized, and do not seem to affect the overall behavior of the tropical cyclone.

VII. SUMMARY

The influence of various SST distributions on the intensities and paths of translating tropical cyclones has been investigated using a three dimensional model of tropical cyclones with improved parameterization of the ABL and Kuo's (1974) cumulus parameterization.

Various distribution of the SST are tested and found to have considerable influence on the intensity and path of the model tropical cyclone (see Table 1). The variations in the SST not only changes the total surface friction, which controls the deflection of the vortex from the mean ambient flow, but also alters the sensible and latent heat exchanges. The magnitude and the spatial distribution of the heat exchanges affect the intensity as well as the movement of the tropical cyclone. Major results are summarized as follows:

1. There is a deflection of approximately five degrees to the right of MAFV as a slowly varying tropical cyclone translates on an f-plane with mean flow over an ocean of uniform SST.
2. The intensity and the angle of deflection increases with increased SST due to enhanced evaporation and friction.
3. When translating downwind the mean flow over the ocean with SST gradients perpendicular to the MAFV, tropical cyclones tend to move into the region of warmer SST. The movement toward warm SST is gradual and continuous.
4. Tropical cyclones are more likely to intensify when warmer ocean situates to the right (left) of the storm track than to the left (right) in the Northern (Southern) Hemisphere because of the asymmetries associated with translating tropical cyclones.

5. Narrow (as compared to the storm size) regions of warmer or cooler SST have little influence on the paths of tropical cyclones. However, if the central portion of the tropical cyclone overlays the narrow region of warm (cooler) SST over a period of time (> 12 h), the tropical cyclone intensifies (weakens).

From these results, we conclude that the SST distribution affects the behavior of a translating tropical cyclone, both frictionally and thermally. In agreement with the adiabatic linear theories, the translating tropical cyclone appears to deflect more to the right of the mean flow when friction is increased (either due to increased surface instability or stronger intensity). The SST distribution also redistributes the available latent energy. This causes a shift in cumulus heating, provides a favorable condition for the growth of the tropical cyclone, and ultimately shifts the vortex toward the warm ocean.

In light of these results, an increased effort to obtain and utilize accurate SST data in operational forecast of tropical cyclones deserves more serious consideration.

ACKNOWLEDGEMENTS

We thank Drs. Winston C. Chao, Mark R. Schoeberl, and Darrell F. Strobel for comments on the manuscript, and Mrs. Jane Polson for typing the manuscript. The research is supported by the Office of Naval Research and the Naval Research Laboratory Contract N00173-78-C-426.

REFERENCES

- Anthes, R. A., 1972: Development of asymmetries in a three-dimensional numerical model of the tropical cyclone. Mon. Wea. Rev., 100, 461-476.
- Anthes, R. A. 1977: A cumulus parameterization scheme utilizing a one-dimensional cloud model. Mon. Wea. Rev., 105, 270-286.
- Anthes, R. A., and S. W. Chang, 1978: Response of the hurricane boundary layer to changes of sea surface temperature in a numerical model. J. Atmos. Sci., 35, 1240-1255.
- Anthes, R. A., and J. E. Hoke, 1975: The effect of horizontal divergence and the latitudinal variation of the Coriolis parameter on the drift of a model hurricane. Mon. Wea. Rev., 103, 757-763.
- Anthes, R. A., S. L. Rosenthal, and J. W. Trout, 1971: Preliminary results from an asymmetric model of the tropical cyclone. Mon. Wea. Rev., 99, 744-758.
- Black, P. G., 1972: Some Observations from Hurricane Reconnaissance Aircraft of Sea-Surface Cooling Produced by Hurricane Ginger (1971). Mariner's Weather Log, 64, 283-298.
- Brand, S., 1971: The effects of tropical cyclone of cooler surface waters due to upwelling and mixing produced by a prior tropical cyclone. J. Appl. Meteor. 10, 865-874.
- Chang, S. W., 1979: The response of an axisymmetric model tropical cyclone to local variations of sea surface temperature. Mon. Wea. Rev., 107, 662-666.

- Chang, S. W. and R. A. Anthes, 1979: The mutual response of the tropical cyclone and the ocean. J. Phys. Oceanogr., 9, 128-135.
- Delsole, F. K. Miyakoda, and R. H. Clarke, 1970: Parameterized processes in the surface boundary layer of an atmospheric circulation model. Quart. J. Roy. Meteor. Soc., 97, 181-208.
- Fisher, E. L., 1958: Hurricane and the sea-surface temperature field. J. Meteor., 15, 328-333.
- Gray, W. M., 1979: Hurricanes: their formation, structure, and likely role in the tropical circulation. Quart. J. Roy. Soc. Meteor., 155-217.
- Jones, R. W. 1977a: Vortex motion in a tropical cyclone model. J. Atmos. Sci., 32, 1518-1527.
- Jones, R. W., 1977b: A nested grid for a three-dimensional model of a tropical cyclone. J. Atmos. Sci., 34, 1538-1553.
- Kuo, H. L., 1969: Motions of vortices and circulating cylinder in shear flow with friction. J. Atmos. Sci., 26, 390-398.
- Kuo, H. L., 1974: Further studies of the parameterization of the influence of cumulus convection on large scale flow. J. Atmos. Sci., 31, 1232-1240.

- Leipper, D. F., and D. Volgenau, 1972; Hurricane Heat Potential of Gulf of Mexico. J. Phys. Oceanogr., 2, 218-224.
- Madala, R. V. and S. A. Piacsek, 1975: Numerical simulation of asymmetric hurricane on a β -plane with vertical shear. Tellus, 27, 453-468.
- Miller, B. I., 1958: On the maximum intensity of hurricanes, J. Meteor., 15, 184-195.
- Moss, M. S., and F. J. Merceret, 1976: A note on several low-layer features of hurricane Eloise (1975). Mon. Wea. Rev., 104, 967-971.
- Ooyama, K., 1969: Numerical simulation of the life cycle of tropical cyclones. J. Atmos. Sci., 26, 3-40.
- Palmen, E., 1948: On the formation and structure of tropical hurricanes, Geophysics, 3, 26-38.
- Perlroth, I., 1967: Hurricane behavior as related to oceanographic environmental conditions. Tellus, 19, 258-267.
- _____ 1969: Effects of oceanographic media on equatorial Atlantic hurricanes. Tellus, 21, 230-240.
- Ramage, C. S., 1972: Interaction between tropical cyclones and the China Sea. Weather, 27, 484-494.

- Ramage, C. S., 1974: The typhoons of October 1970 in the South China Seas: Intensification, decay, and ocean interaction. J. Appl. Meteor., 13, 739-751.
- Rosenthal, S. L., 1971: The response of a tropical cyclone model to variations in boundary layer parameters, initial conditions, lateral boundary conditions, and domain size. Mon Wea. Rev., 99, 767-777.
- Sheets, R. C., 1969: Some mean hurricane soundings J. Appl. Meteor., 8, 134-146.
- Sundqvist, H., 1972: Mean tropical storm behavior in experiments related to modification attempts. Tellus, 24, 6-12.
- Tisdale, C. F., and P. F. Clapp, 1963: Origin and paths of hurricanes and tropical storms related to certain physical parameters at the air-sea surface. J. Appl. Meteor., 2, 358-367.

FOOTNOTES

1. Madala, R. V., and S. W. Chang, 1979: A vectorized three-dimensional operational tropical cyclone model. Preprint Scientific Computer Information Exchange Conference, August 1979, Livermore.
2. Chang, S. W. and R. V. Madala, 1980: Planetary boundary layer parameterization for tropical cyclones based on generalized similarity theory. Naval Research Laboratory Memorandum Report 4235. Available at Code 4780, NRL, Washington, DC 20375.
3. The areal sum of the vertically integrated heat content above some critical temperature.

LIST OF FIGURES

1. The vertical structure of the numerical model of the tropical cyclone.
2. The boundary layer wind vector and surface pressure at 84 h of the control equipment (Exp. A).
3. The surface stress (dyne cm^{-2}) at 84 h of Exp. A. Dotted line is 1 dyne cm^{-2} contour, solid lines are 2.5, 5.0, 7.5, ..., etc. dyne cm^{-2} .
4. The evaporation rate (cm day^{-1}) at 84 h of Exp. A. Dotted lines are 0.5 cm day^{-1} , solid lines are 1, 2, ..., etc. cm day^{-1} .
5. The various SST distributions tested.
6. The time series of the minimum pressures of Exps. A, W, and C.
7. The time series of the maximum surface winds of Exps. A, W, and C.
8. The paths of storm centers for Exps. A, W, and C. The numbers in curves denote times in an hour. The numbers on coordinates are grid points.
9. The evaporation rate at 27 h of Exp. W.
10. The time series of the minimum pressures of Exps. A, WR, and WL.
11. The time series of the maximum surface winds of Exps. A, WR, and WL.
12. Same as Figure 8, except for Exps. A, WR, and WL.
13. The wind vectors at $\sigma = 0.66$ level, the surface pressure field in mb (solid lines), and the evaporation rate in cm day^{-1} (dash lines) near the storm center for Exp. WR at 48 h.
14. Same as Figure 13 except for Exp. WL.
15. The time series of the minimum pressures of Exps. A, WS, and CS.
16. The time series of the maximum surface winds of Exps. A, WS, and CS.
17. Same as Figure 8 except for Exps. A, WS, and CS. The shaded area is the strip of warm or cold SST.
18. The evaporation rate (cm day^{-1}) at 30 h of Exp. WS. Shaded area is the warm strip.

APPENDIX C

TEST OF A
PLANETARY BOUNDARY LAYER PARAMETERIZATION
BASED ON A GENERALIZED SIMILARITY THEORY
IN TROPICAL CYCLONE MODELS

TEST OF A
PLANETARY BOUNDARY LAYER PARAMETERIZATION
BASED ON A GENERALIZED SIMILARITY THEORY
IN TROPICAL CYCLONE MODELS

by

Simon Wei-jen Chang
JAYCOR
Alexandria, VA. 22304

October, 1980

ABSTRACT

A planetary boundary layer (PBL) parameterization based on the generalized similarity theory (GST) was tested in tropical cyclone models. This parameterization, with only one layer, is desired in modeling tropical cyclones for computational speed. The momentum, sensible heat and moisture fluxes are mutually dependent in this parameterization through non-dimensional gradient equations. The internal structure of the PBL is determined implicitly through universal functions.

In comparison with a complex, one-dimensional, multi-layer PBL model, the GST parameterization yields accurate moisture fluxes, but slightly overestimates the momentum flux and underestimates the sensible heat flux. The GST parameterization produces very realistic dynamics, energetics and thermal structure in an axisymmetric tropical cyclone model. This GST parameterization, although unable to treat the diffusion across the PBL inversion, is judged superior to drag coefficient parameterization and is a good alternative to the more expensive, multi-layer parameterization.

I. INTRODUCTION

The planetary boundary layer (PBL) plays a critical role in the evolution of tropical cyclones because the air-sea energy and momentum exchanges occur through the PBL. Parameterization of the PBL is thus a very important aspect of tropical cyclone modeling. Complex parameterization is not always computationally feasible for three-dimensional or operational models. Computationally efficient yet accurate PBL parameterization is imperative for these models. The purpose of this paper is to test such a parameterization based on the generalized similarity theory (GST) in the parameterization of the PBL in tropical cyclone models.

The most widely used PBL model is the single-layer parameterization where the PBL is represented by one model layer and the surface fluxes are calculated using bulk aerodynamic formulas. This method is simple and computationally economical but has a major drawback in that the internal structure of the PBL cannot be resolved. As a consequence, the single layer PBL model using bulk aerodynamic formulas can only crudely estimate various surface fluxes.

An alternative approach where the PBL is modeled by several layers has been adopted in recent years by Pielke (1974), Kurihara and Tuleya (1974), Anthes and Chang (1978) and Anthes and Warner (1978). By explicitly resolving the PBL structure, these models often yield more realistic estimates of the various fluxes, but the computational cost is high.

Recent observational studies have facilitated the testing of various PBL similarity theories. The rather idealized assumptions characteristic of early theories have been relaxed and improved, and more realistic and general theories have been derived (Arya 1977; Yamada, 1976). These developments have led to a PBL formulation that appears suitable to model various PBL conditions.

In the next section, a brief review of the generalized similarity theory will be given. In Section 3, various surface fluxes in typical tropical cyclone conditions obtained from the GST will be compared with those computed by a time dependent one dimensional PBL model (Busch, et al., 1976; hereafter referred as BCA). The generalized similarity theory is then applied to an axisymmetric tropical cyclone model. The results will be compared in Section 4 with those obtained using constant drag coefficients.

II. GENERALIZED SIMILARITY THEORY

Similarity theory states that the profile of any properly scaled variable in the PBL such as wind, temperature, or water vapor, can be described by a universal function. Although there has been much debate concerning the proper scales for the various types of PBL's (Arya, 1977) we will use a similarity theory that appears most applicable and general for tropical cyclones (Yamada, 1976).

The mathematical representation of the PBL flow can be obtained by assuming that there exists a layer where both the equations describing the surface layer and the equations describing the interior flow in the mixed layer are both valid. In the surface layer, the PBL variables are assumed to follow a logarithmic-linear relationship with height:

$$\hat{t} \frac{|\tilde{v}|}{u_*} = \frac{\hat{t}}{k} \left[\ln \left(\frac{z}{z_0} \right) - \psi_m \left(\frac{z}{L} \right) \right] \quad (1a)$$

$$\frac{\theta - \theta_0}{\theta_*} = \left[\frac{P_r}{k} \ln \left(\frac{z}{z_0} \right) - \psi_h \left(\frac{z}{L} \right) \right] \quad (1b)$$

$$\frac{q - q_0}{q_*} = \frac{P_r}{k} \left[\ln \left(\frac{z}{z_0} \right) - \psi_q \left(\frac{z}{L} \right) \right] \quad (1c)$$

where \hat{t} is the unit vector parallel to the surface wind, P_r is the turbulent Prandtl number, ψ_m , ψ_h , and ψ_q are stability functions, z_0 is the roughness length, and θ_0 and q_0 are potential temperature and specific humidity at z_0 .

For the interior flow in the mixed layer we can write the equations in the form of the resistance law:

$$\frac{V-V_m}{u_*} = \hat{t} F_u\left(\frac{z}{h}, \frac{h}{L}\right) + \hat{n} F_v\left(\frac{z}{h}, \frac{h}{L}\right) \text{ sign } f \quad (2a)$$

$$\frac{\theta-\theta_m}{\theta_*} = F_\theta\left(\frac{z}{h}, \frac{h}{L}\right) \quad (2b)$$

$$\frac{q-q_m}{q_*} = F_q\left(\frac{z}{h}, \frac{h}{L}\right) \quad (2c)$$

where V_m , θ_m and q_m are the mean velocity, potential temperatures and water vapor content in the PBL, \hat{n} is a unit vector normal to \hat{t} , h is the height of the PBL, F_u , F_v , F_θ , and F_q are functions to be determined.

Assuming a matching layer where (1) and (2) are simultaneously valid, one can obtain a relation between the surface fluxes and the average PBL parameters:

$$\frac{ku_m}{u_*} = \ln\left(\frac{h}{z_0}\right) - A\left(\frac{h}{L}\right) \quad (3a)$$

$$\frac{kv_m}{u_*} = -B\left(\frac{h}{L}\right) \text{ sign } f \quad (3b)$$

$$\frac{k(\theta_0-\theta_m)}{P_r\theta_*} = \ln\left(\frac{h}{z_0}\right) - C\left(\frac{h}{L}\right) \quad (3c)$$

$$\frac{k(q_0-q_m)}{P_rq_*} = \ln\left(\frac{h}{z_0}\right) - D\left(\frac{h}{L}\right) \quad (3d)$$

where u_m and v_m are the components of the mean velocity in the PBL in t and n directions, respectively. Universal functions A, B, C, and D determined empirically. It is generally assumed that $D \approx C$ (see Arya, 1977).

Using equation set (3), and the Wagara observational data, Yamada (1976) obtained functions A, B, and C (eqs. (13) through (18) in his paper) which are adopted here because of the simple functional form and accuracy.

It should be noted that \bar{V}_m in Yamada's analysis is the vertically averaged geostrophic wind in the PBL. Here \bar{V}_m is the vertically averaged mean wind. Thus the baroclinic effects are minimized (Arya, 1978). In addition, when actually applying Eq. (3) in a dynamic model, the sum of the squares and the quotients of Eqs. (3a) and (3b) are used to evaluate the magnitude and direction of the surface wind stress.

III. GENERALIZED SIMILARITY THEORY AND MULTI-LAYER APPROACHES IN A ONE DIMENSIONAL TROPICAL CYCLONE MODEL

As stated in the introduction, the parameterization of the PBL based on the GST for a tropical cyclone model is very appealing because it requires only one layer to represent the PBL. Thus it is important to test the universal functions described by Eq. (3) with the observations of tropical cyclones. Unfortunately, detailed observations of tropical cyclone PBL's are not yet available, so we resort to use a one-dimensional, multi-layer PBL model for comparison. Table 1 lists various models used in this study.

The BCA 1-D PBL model can reproduce observations accurately and it has been used successfully in parameterizing the PBL in numerical models (Anthes and Chang, 1978; Anthes et al., 1978). The model has a surface layer in which the logarithmic-linear relationships for wind and temperature (Businger et al., 1971) are adopted. It should be noted that the same logarithmic-linear relationship is used by Yamada (1976) to generate the universal functions. Above the surface layer, a time dependent mixing length is used. The mixing length is assumed to continuously approach its asymptotic value, which depends on the depth and stability of the PBL. The e-folding time of the mixing length is proportional to the size of the energy-containing eddies in the PBL and inversely proportional to the turbulent kinetic energy.

The 1D version of the BCA model used in this study has 20 layers using a stretched grid from the surface to 3 km. The lowest layer defined as the surface layer, has a thickness of 25 m. To properly simulate tropical cyclone condition, a rather strong pressure gradient

TABLE 1
Model Used For Comparison

Models	Type	Dimensions	PBL Parameterization
GST	PBL	1	Single-layer generalized similarity theory
BCA	PBL	1	Multi-layer, Busch et al. (1976)
S	Tropical Cyclone	2	Single-layer, generalized similarity
D1	Tropical Cyclone	2	Single-layer, $C_D = 0.0015$ $C_E = C_H = 0.003$
D2	Tropical Cyclone	2	Single-layer, $C_D = 0.003$ $C_E = C_H = 0.003$
M	Tropical Cyclone	2	Multi-layer, Busch et al.

force is specified so that the geostrophic wind speed is strongest at the surface and decreases with height to 90% of its surface strength at 3 km. The initial thermal state which has been taken from the model hurricane of Anthes and Chang (1978) shows a well mixed PBL below a capping inversion at 600 m with a sharp increase of potential temperature and decrease of specific humidity above the inversion. The initial wind is equal to the geostrophic wind prescribed for each run.

The BCA model was integrated 12 hours for 24 cases with the values of the geostrophic wind set at 15, 25 and 35 m s⁻¹ and the sea-surface temperature (SST) varying from 24.4 to 29.4°C. These variations produce different stability conditions and large rates of change in the initial hours. Diagnoses using Eq. (3) (or GSA model) were given at model times of 1, 2, 3, 4, 6, 8, 10, and 12 h. The vertically integrated u , v , θ , and q in the BCA model are the mean PBL properties needed for the diagnoses. Figure 1 shows the comparison of the surface wind stresses between the diagnoses from GST model and the computation of BCA model. The GST model produced nearly the same results (points on the diagonal line in Figure 1) as the BCA model for small u_*^2 value and for the unstable conditions. The stress diagnosed by the GST are higher than the BCA model under stable conditions. The overestimate by the GST model lessens as instability increases.

The larger estimation of the surface stresses for stable conditions of the GST model is due to the greater wind shear in the lower PBL which is resolvable in the BCA model. This strong wind shear is not properly represented by the universal functions in the single layer approach. When such a strongly sheared layer, which usually accompanies

a low-level inversion, is present, the PBL mean wind may not be a proper velocity scale for the PBL. Fortunately, the formation of such a low-level inversion is not likely in tropical cyclones, the GST model therefore seems to estimate the momentum fluxes in typical tropical cyclones quite well.

We used a constant aerodynamic drag coefficient of 1.5×10^{-3} to estimate the stresses based on the surface winds from the BCA model. Because the drag coefficient is independent of stability, the value of the stresses depends strongly on the wind speed. A comparison with BCA model shows that most of the values cluster along the three horizontal lines and scatter within the vertical bars on two ends of each line in Figure 1. These scattering and clustering points are also typical for the drag coefficient model in heat flux and moisture flux. It is apparent that the stresses of the GSA model have more correlation and less scattering to those of the more sophisticated BCA model as compared to the aerodynamic drag coefficient model.

Figure 2 and Figure 3 show the comparisons of the upward and downward sensible heat fluxes, respectively. For unstable conditions, The GST model underestimates the upward heat flux because of the formation of a strong superadiabatic lapse rate region near the surface in the BCA model. For stable conditions the GST model overestimates the downward heat flux. This is related to the formation of low-level inversion in the BCA model which effectively cuts off the downward transport of heat. These characteristics of the GST model are found in almost all single-layer parameterizations because the strong gradient in lower PBL cannot be resolved. This difficulty cannot be easily

AD-A098 635

JAYCOR ALEXANDRIA VA

F/6 4/2

DEVELOPMENT OF A PBL PARAMETERIZATION SCHEME FOR THE TROPICAL C--ETC(U)

MAR 81 S W CHANG, C AGRITELLIS

N00173-79-C-0465

UNCLASSIFIED

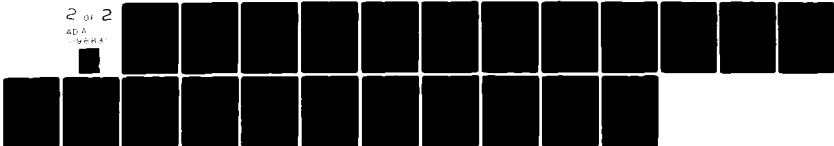
JAYCOR-PSD-200-81-004FR

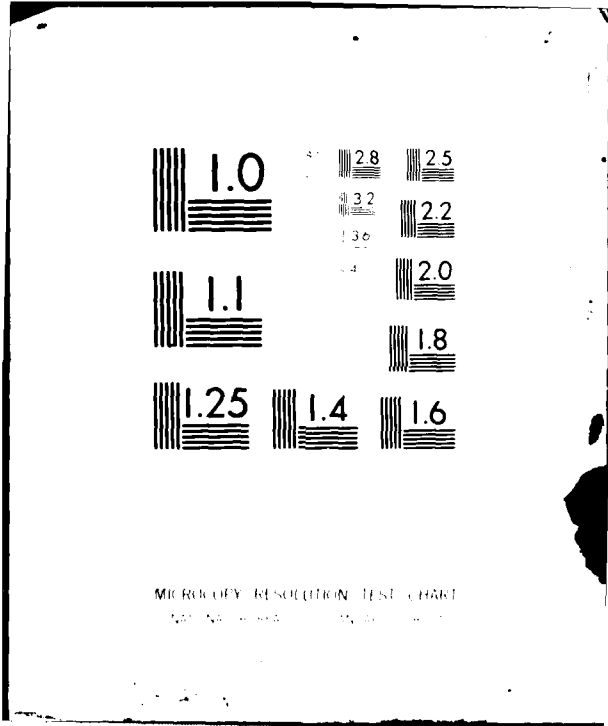
NL

2 of 2

AD-A

79-614





MICROCOPY RESOLUTION TEST CHART
NATIONAL BUREAU OF STANDARDS - 1963-A

overcome when a single-layer PBL has to be employed in a numerical model for economic reasons.

Figure 4 shows the comparison of the moisture flux $\overline{w'q'}$. The GST model gives a higher $\overline{w'q'}$ for the unstable condition, and a very similar $\overline{w'q'}$ for near neutral conditions, and scattering in Fig. 4 is similar to that in Fig. 1, the more symmetric distribution about the diagonal in Fig. 4 is presumably related to the larger value of $\frac{\partial q}{\partial z}$ in the lower part of the BCA model.

These deviations of the GST model from the BCA model are much less than the model using aerodynamic drag coefficients. Using a constant drag coefficient, various fluxes depend almost solely on the wind speed. The deviations of the GST model from the BCA model is partially inherited from the scattering of the original observation data from which the universal functions are deduced (Yamada, 1976). The comparison, however, does indicate a distinct behavior of the GST model for different stability. It should be pointed out that the GST has been applied to highly non-stationary conditions in this analysis. We note that as the PBL approaches a quasi-steady state, the GST model diagnoses becomes comparable to the BCA model results.

The experiments with the one-dimensional model indicates that the GST model agrees very well with the Busch model in momentum and moisture flux predictions. The GST model does not predict accurate fluxes when there are strong low-level gradients of potential temperature. The surface heat flux, however, is fortuitously not critically important in the development and maintenance of tropical cyclones as pointed out

by Rosenthal (1971) and Anthes and Chang (1978). The single layer approach with GST model in parameterizing the PBL in a tropical cyclone is thus adequate.

IV. INCORPORATION WITH AN AXISYMMETRIC TROPICAL CYCLONE MODEL

A. Model Review

The axisymmetric tropical cyclone model used for our investigation is similar to the one described in Anthes and Chang (1978) except that (1) the finest resolution at small radii is 30 km, and (2) there are six vertical layers. The vertical σ -layers are bounded at levels $\sigma = 0.0, 0.2, 0.3, 0.6, 0.8, 0.93$, and 1.

Included in one earlier version of the model was a time dependent equation for the PBL height similar to that in Deardorff (1972). Supplementary experiments showed that the equation predicts infinite growth of PBL near the center of the cyclone unless large horizontal diffusion is applied. We, therefore, hold the height of PBL constant between $\sigma = 0.93$ and 1. The PBL has a depth of 650 = 700 m, a typical observed PBL depth near tropical disturbances (Moss and Merceret, 1976; Nitta, 1974). Charnock's equation (Delsol et al., 1970) is used to compute the roughness length. The initial conditions consist of a weak vortex, which is in gradient balance, with maximum tangential velocity of 17 m s^{-1} , embedded in a tropical atmosphere (Jordon, 1958). The lateral boundary conditions are Dirichlet for the thermodynamic variables and zero-vorticity for the momentum.

For comparison purposes models were integrated using constant drag coefficients with $C_D = 0.0015$, $C_H = 0.003$ (model D1) and with $C_D = 0.003$, $C_H = C_E = 0.003$ (model D2). A nine-layer tropical cyclone model (model M), identical to that of Anthes and Chang (1978) except for the 30 km horizontal resolution, is also integrated.

B. Development into Tropical Cyclones

The development from the initial vortex into a tropical cyclone is depicted by the maximum surface wind (Fig. 5) and minimum pressure (Fig. 6). After the initial dissipation due to friction, Model S rapidly develops into an intense cyclone and reaches a quasi-steady state at about 40 hr. The maximum surface wind is about 57 m s^{-1} and the minimum surface pressure is approximately 958 mb.

Models D1 and D2 also intensify after the initial dissipation stage. These two models deviate considerably from each other and from Model S after 20 h. Model D1 reaches a final intensity of 35 m s^{-1} and 986 mb, whereas Model D2 reaches a final intensity of 43 m s^{-1} and 980 mb. Model M behaves in a very similar fashion as Model S, exemplified by the continuing intensification between 20 to 40 h and the final intensity of 52 m s^{-1} wind and 956 mb pressure.

C. Cyclone Structure at Quasi-Steady State

The tangential velocity field at 48 h for Model S shows a strong and concentrated cyclonic circulation near the center (Fig. 7). The maximum velocity is at $r = 30 \text{ km}$ in the lowest level and the 40 m s^{-1} contour extends upward to $\sigma = 0.6$. The tangential circulation diminishes upward due to the baroclinic effect of the warm core and anticyclonic circulation occurs at the $\sigma = 0.2$ level outside of 300 km. The inflow is confined to the PBL with maximum radial velocity of 35 m s^{-1} just outside the region of the maximum tangential velocity (Fig. 8). Strong outflow with velocity more than 20 m s^{-1} occurs at the $\sigma = 0.2$ level. Except for the shallow inflow and outflow layers, the radial velocity is small in mid-troposphere.

Figure 9 shows the relative humidity (RH) at 48 h of Model S. The RH field features (1) very moist PBL and outflow canopy, (2) relative moist convective eyewall region, (3) a dry eye region due to the strong sinking motion, and (4) a dry mid-troposphere outside the eyewall due to the general subsidence.

The temperature field of the quasi-steady tropical cyclone shows a warm core with an anomaly of more than +12°C. The +8°C anomaly extends to $r = 300$ km in the outflow layer. The +2°C anomaly contour between $\sigma = 0.06$ and $\sigma = 0.9$ outlines the subsidence. The cooler PBL near the center is due to the adiabatic expansion (and therefore cooling) in the inflow.

D. Air-Sea Energy Transfer

We will use budget calculations of kinetic energy, moisture, and heat to compare model results and reveal the importance of various physical processes. As shown in Anthes and Chang (1978), the budgets of kinetic energy (K), moisture (Q) and enthalpy (H) for a tropical cyclone model can be expressed schematically by:

$$\frac{\partial K}{\partial t} \approx K_b + C + D_v + D_L + D_H$$

$$\frac{\partial Q}{\partial t} \approx Q_b + E + P + Q_H$$

$$\frac{\partial H}{\partial t} \approx H_b + A + Q_p + H_s + H_H$$

where the terms with subscript b's denote the lateral boundary fluxes, and terms with subscript H's denote the effects due to horizontal

diffusion. In addition, D_V , and D_C represent the rates of kinetic energy dissipation due to surface friction and cumulus friction respectively. E and P denote evaporation and precipitation rates respectively. Q_p represents latent heat release, and H_s the surface sensible heat transfer. A denotes the adiabatic heating rate due to vertical motion; C denotes the kinetic energy conversion rate due to cross-isobaric flow.

Within the model domain of $\sigma = 0$ to 1 and $r = 0$ to 300 km, the most direct contribution of the PBL processes are the air-sea sensible and latent heat exchanges. Figure 11 and 12 show the time series of H_s and E . During the early stages, the sensible and latent heat transfers of D1 are equal or greater than those of S. The sensible and latent heat exchanges in S, however, grow steadily after 10 hr and finally reach $15 \times 10^{12} \text{W}$ and 3 cm d^{-1} respectively, whereas in D1, the sensible and latent heat exchanges only grow to maxima of $7.5 \times 10^{12} \text{W}$ and 1.8 cm d^{-1} after 30 h. After the maxima are reached, they decrease with time because of stabilization and saturation of the PBL.

Apparently, the sensible and latent heat exchanges in S are maintained at high levels primarily due to their nonlinear dependence on wind speed and stability. As wind speed in S approaches its maximum after 30 h, both H_s and E are enhanced to a greater extent than in D1. In addition, the radial circulation in S is also increased so that a slightly unstable and dry PBL is maintained by the strong inflow.

The time variation of E for model M is very close to model S. The sensible heating rate H_s , however, are very different. This is because in model M a downward heat flux across the PBL top is allowed. Anthes and Chang (1978) argued this as an alternative heat source for maintaining the quasi-isothermal hurricane PBL. The GSA does not consider the across inversion mixing, therefore Model S depends on extracting sensible heat from the ocean to maintain its quasi-isothermal inflow layer.

The increased radial circulation is illustrated by the conversion rate C from the available potential energy to kinetic energy shown in Fig. 13. The conversion rate is approximately proportional to the combined strength of the radial circulation and the warm core. It is apparent that the conversion rates in Model S and M grow rapidly between 10 to 20 h, which coincides with the increased evaporation. The proportionally faster increase of C than H_s and E in Model S shows that the increased heat transfer creates a stronger inflow, which, in turn, maintains a stronger heat transfer and a stronger inward transport of the dry, cooler ambient air.

The two different PBL parameterizations also gives different dissipation rates (Fig. 14). Note that D_V in S is smaller before 15 h than in D1, and it eventually asymptotes to three times stronger. Again, this is due to the nonlinear dependence of the surface stress on wind speed.

One can argue that the nonlinear dependence of the air-sea energy exchange could be achieved by employing wind-speed-dependent drag coefficients. However, the parameterization based on similarity theory is superior. The heat and momentum transfers depend not only

on wind speed but also on PBL stability, and it is through PBL stability that various fluxes are correlated. The surface roughness appears in the formulation as a length scale and thus the parameterization captures an important feedback from the sea state. The turning of wind in low levels, neglected in the parameterization with drag coefficient, is also included implicitly. Therefore, the surface stress backs from the direction of the PBL mean wind, as expected.

Overall, the generalized similarity theory is quite similar in estimating surface fluxes to the more sophisticated Busch et al model and appears to be applicable in parameterization of the PBL in the tropical cyclone models. Such parameterization contains several realistic PBL characteristics such as the mutual dependence of various fluxes and the backing of the low-level wind. Although it cannot resolve the strong gradient in a stable PBL nor the across-inversion mixing in some single-layer parameterizations, it is still superior than the parameterization using stability-independent drag coefficient. In cases that a multi-layer parameterization is economically infeasible, the parameterization outlined by (3) is a good alternative.

V. SUMMARY

A PBL parameterization based on the generalized similarity theory has been tested for tropical cyclone models. We conclude that a single layer approach in parameterizing the PBL is viable although it cannot resolve the detailed structure of the PBL.

This parameterization was compared with the 1D multi-level PBL model of Busch et al. (1976) under various stabilities and highly nonstationary conditions. For stationary conditions, the computed water vapor flux, agrees well with the Busch model. The momentum flux is overestimated and the sensible heat flux is underestimated especially when there is a low-level inversion.

An axisymmetric tropical cyclone model which incorporated this single-layer parameterization produced very realistic dynamic and thermodynamic structures. In comparison with otherwise identical tropical cyclone models that employ constant drag coefficients, the superiority of stress-dependent drag coefficients in the development of tropical cyclones was demonstrated.

ACKNOWLEDGEMENTS

The author thanks Dr. R. V. Madala for his support, Drs. M. R. Schoeberl, D. F. Strobel, and R. T. Williams for comment on the manuscript. Sharon Richardson and Jane Polson who diligently typed the manuscript. The research is supported by the Naval Research Laboratory through grant N00173-78-C-0421.

REFERENCES

- Anthes, R. A., and S. W. Chang, 1978: Response of the hurricane boundary layer to changes of sea surface temperature in a numerical model. J. Atmos. Sci., 35, 1240-1255.
- Anthes, R. A., and T. T. Warner, 1978: Development of hydrodynamic models for air pollution and other mesometeorological studies. Mon. Wea. Rev., 106, 1045-1078.
- Arya, S. P. S., 1978: Comparative effects of stability, baroclinicity and the scale-height ratio on drag laws for the atmospheric boundary layer. J. Atmos. Sci., 35, 40-46.
- Arya, S. P. S., 1977: Suggested revisions to certain boundary layer parameterization schemes used in atmospheric circulation models. Mon. Wea. Rev., 105, 215-227.
- Busch, N. E., S. W. Chang, and R. A. Anthes, 1976: A multi-level model of the planetary boundary layer suitable for use with mesoscale dynamic models, J. Appl. Meteor., 15, 909-919.
- Businger, J. A., J. C. Wyngaard, Y. Izumi, and E. F. Bradley, 1971: Flux profile relationships in the atmospheric surface layer. J. Atmos. Sci., 28, 181-189.
- Delsol, F., K. Miyakoda, and R. H. Clarke, 1970: Parameterized processes in the surface boundary layer of an atmospheric circulation model. Quart. J. Roy. Meteor. Soc., 97, 181-208.
- Jordan, C. L., 1958: The thermal structure of the core of tropical cyclones. Geophysics, 6, 218-297.

- Kurihara, Y., and R. E. Tuleya, 1974: Structure of a tropical cyclone developed in a three-dimensional numerical simulation model. J. Atmos. Sci., 31, 893-919.
- Moss, M. S., and F. J. Merceret, 1976: A note on several low-layer features of Hurricane Eloise (1975). Mon. Wea. Rev., 104, 967-971.
- Pielke, R. A., 1974: A comparison of three-dimensional and two-dimensional numerical predictions of sea breezes. J. Atmos. Sci., 31, 1577-1585.
- Rosenthal, S. L., 1971: The response of a tropical cyclone model to variations in boundary layer parameters, initial conditions, lateral boundary conditions, and domain size. Mon. Wea. Rev., 99, 767-777.
- Yamada, T., 1976: On the similarity functions A, B, and C of the planetary boundary layer. J. Atmos. Sci., 33, 781-793.

FIGURES

1. Surface stresses (m^2s^{-1}) computed by generalized similarity theory versus those computed by the 1D PBL model for stable (\bullet), unstable (\circ), and neutral (m) conditions. Points should fall on the diagonal line if two models agree.
2. Same as Figure 1 except for upward surface heat flux in unstable condition (C m s^{-1}).
3. Same as Figure 1 except for downward surface heat flux in stable conditions (C m s^{-1}).
4. Same as Figure 1 except for surface vapor flux ($\text{g g}^{-1} \text{m s}^{-1}$).
5. Time series of the maximum winds for models S, D1, D2, and M.
6. Time series of the minimum surface pressures for models S, D1, D2, and M.
7. The quasi-steady tangential velocity (m s^{-1}) of model S at 48 h. Positive values denote cyclonic circulation, negative values denote anticyclonic circulation.
8. The quasi-steady radial velocity (m s^{-1}) of model S at 48 h. Positive values denote outflow, negative values denote inflow.
9. The quasi-steady relative humidity (%) of Model S at 48 h.
10. The quasi-steady temperature anomalies (C) of Model S at 48 h. The anomalies are defined as temperature departures from the initial state.
11. Time series of surface heat flux from $r = 0$ to 300 km of models S, D1, and M.
12. Same as Figure 11 except for averaged evaporation rate.
13. Same as Figure 11 except for KE conversion rate.
14. Same as Figure 11 except for KE dissipation rate due to surface friction.

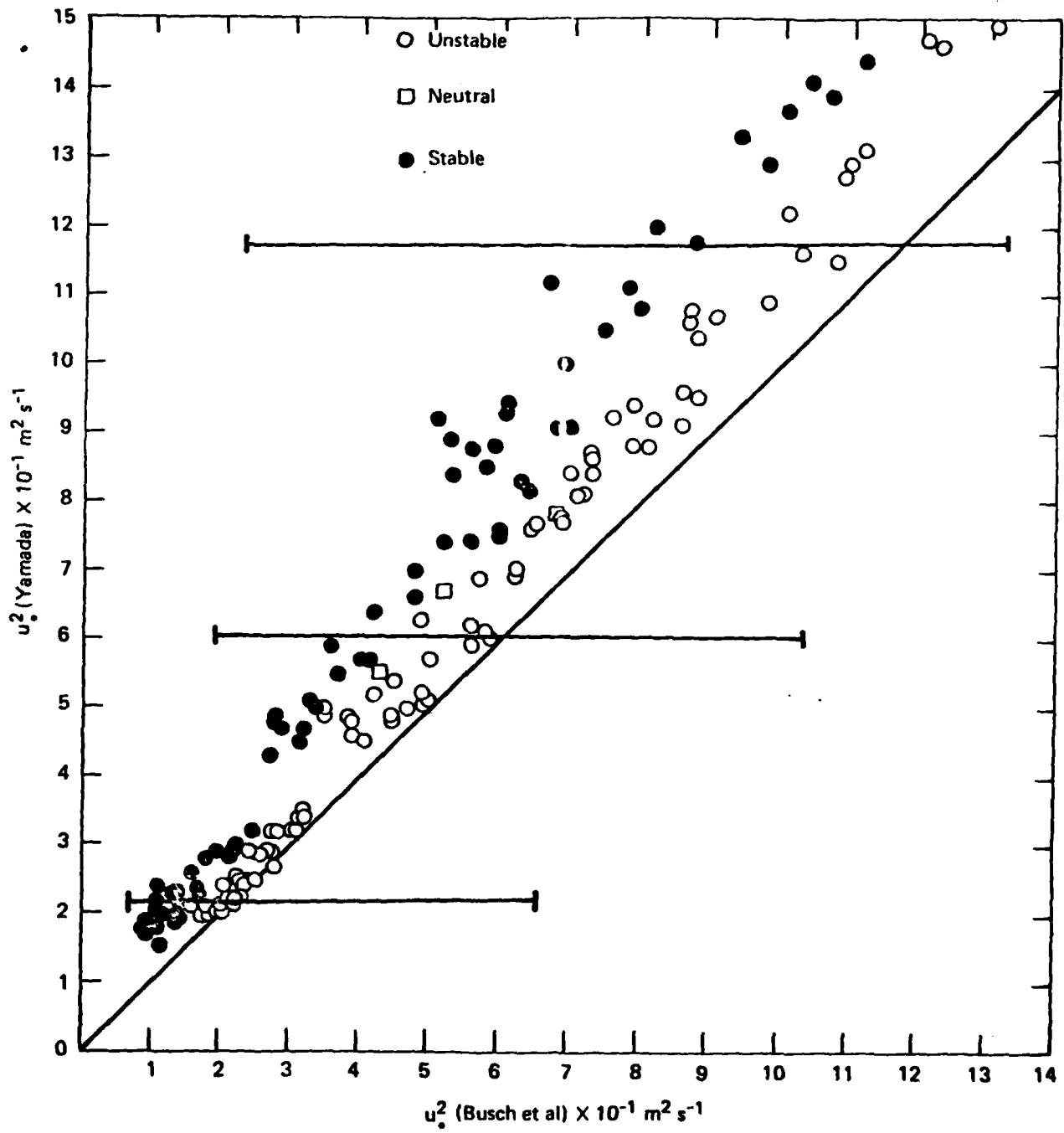


Figure 1

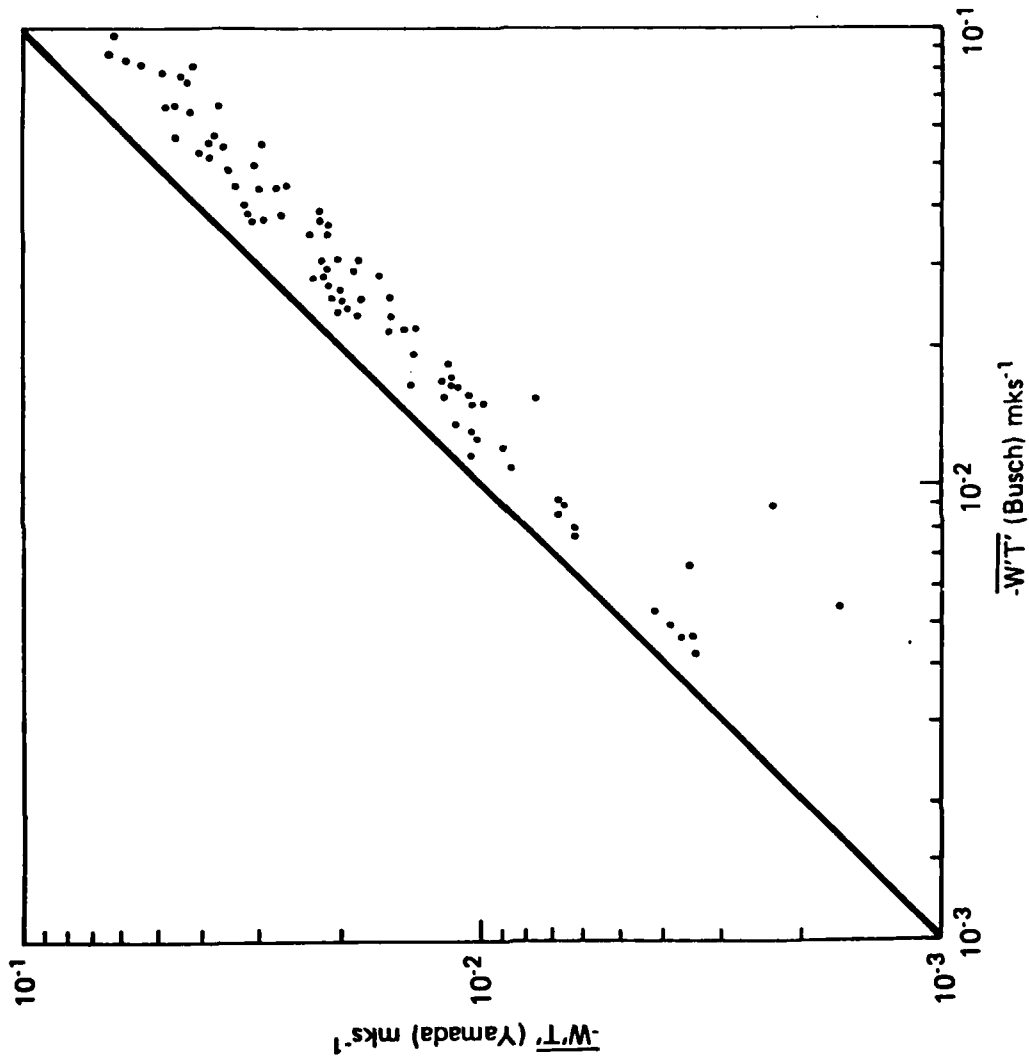


Figure 2

11-1-55

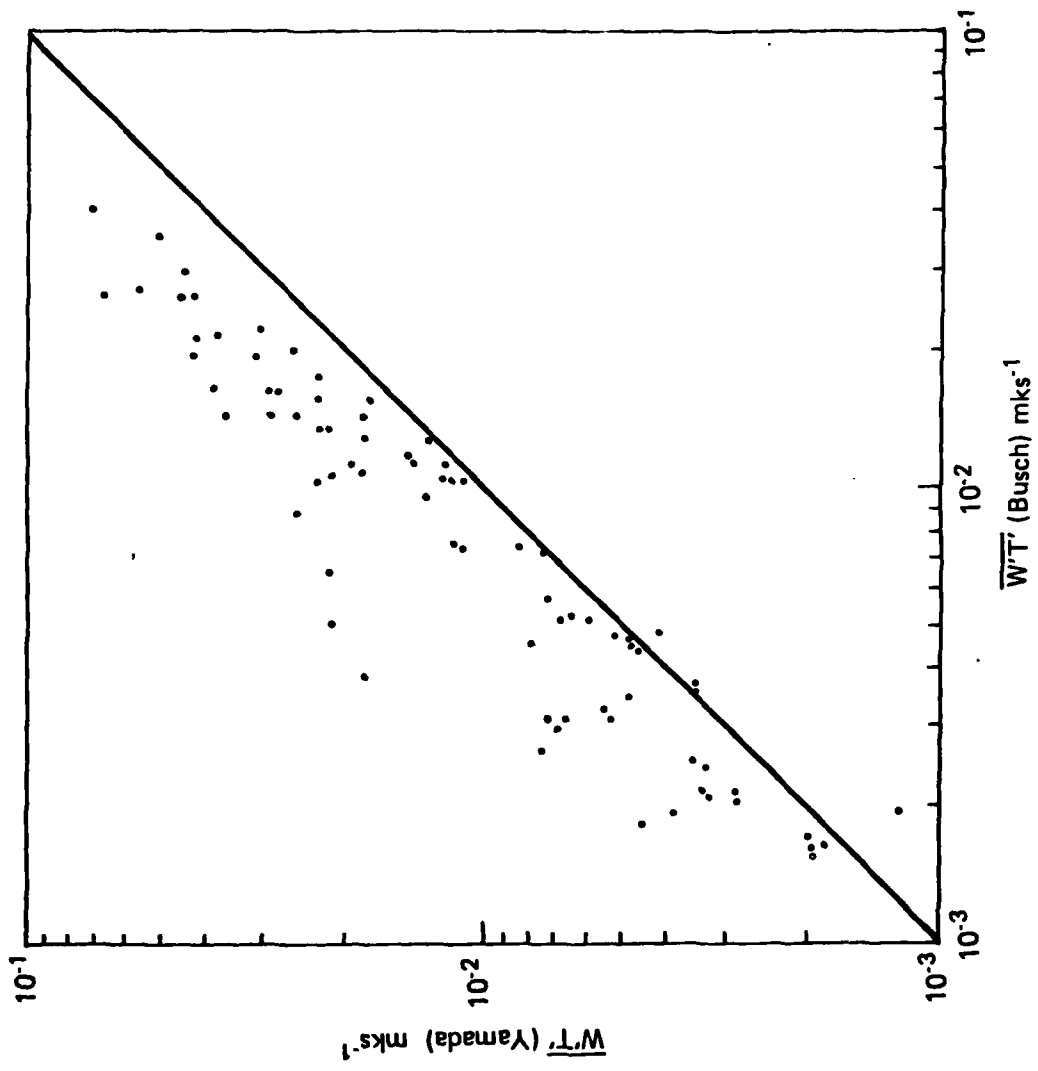


Figure 3

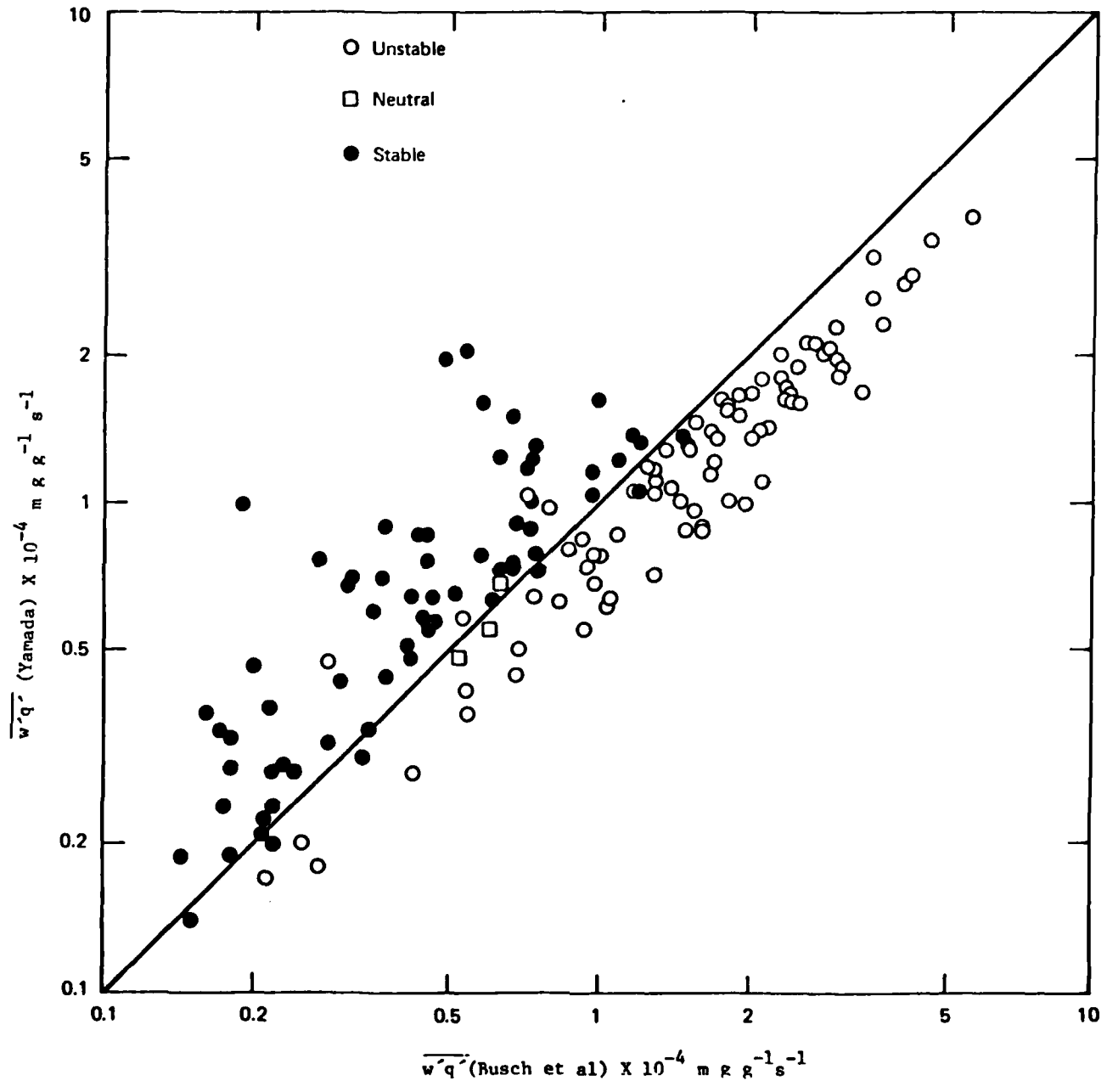


Figure 4

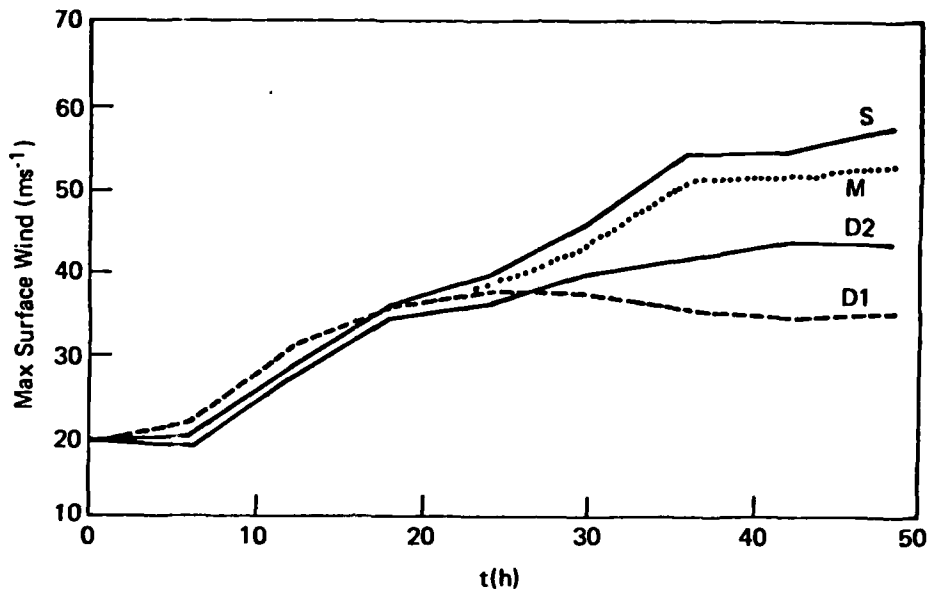


Figure 5

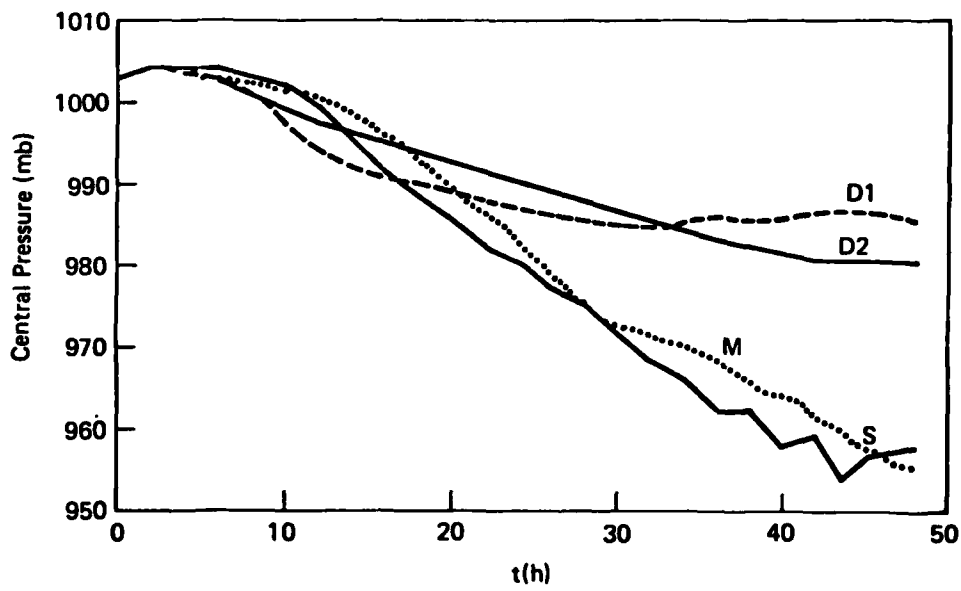


Figure 6

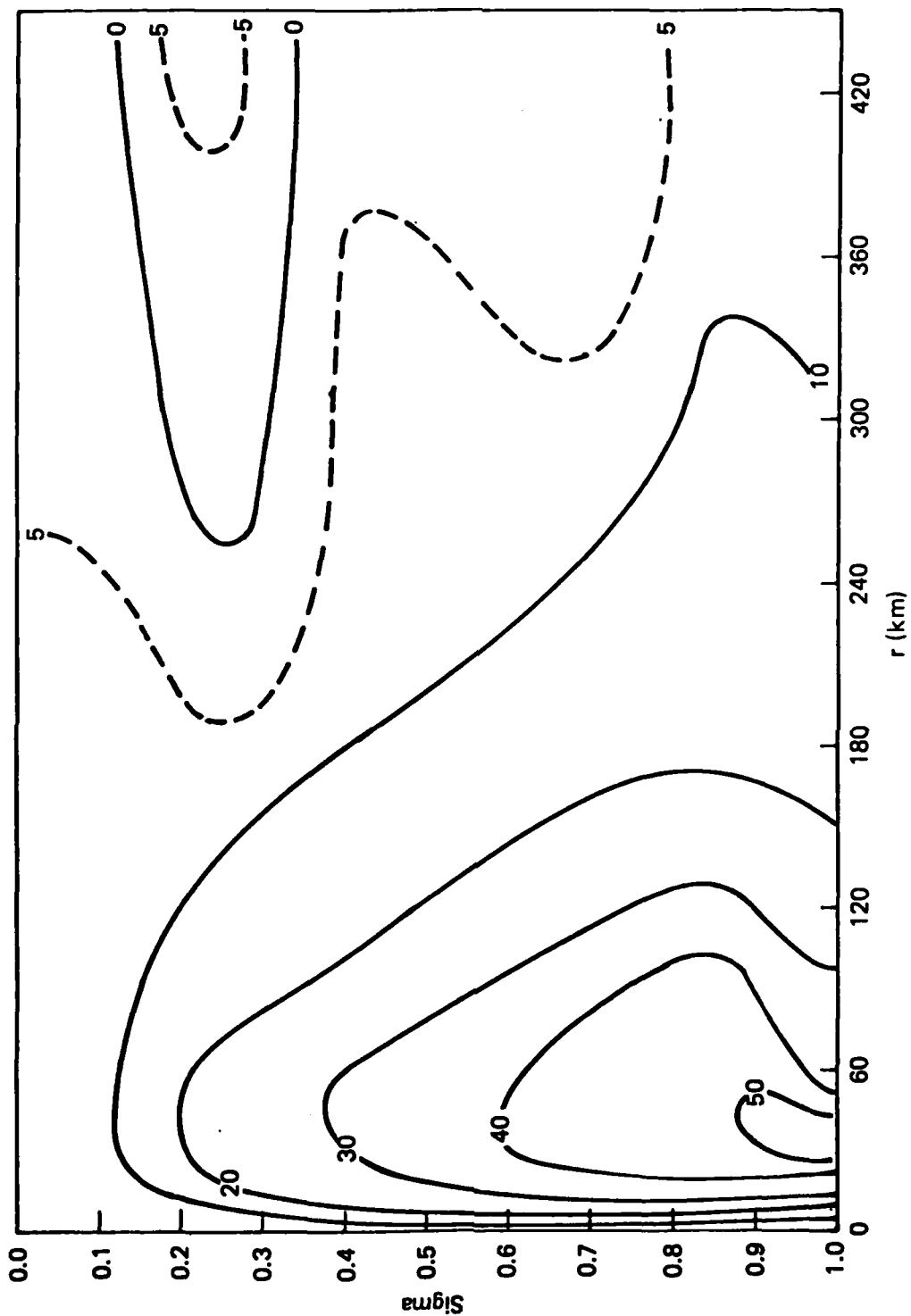


Figure 7

186
1. 9. 5

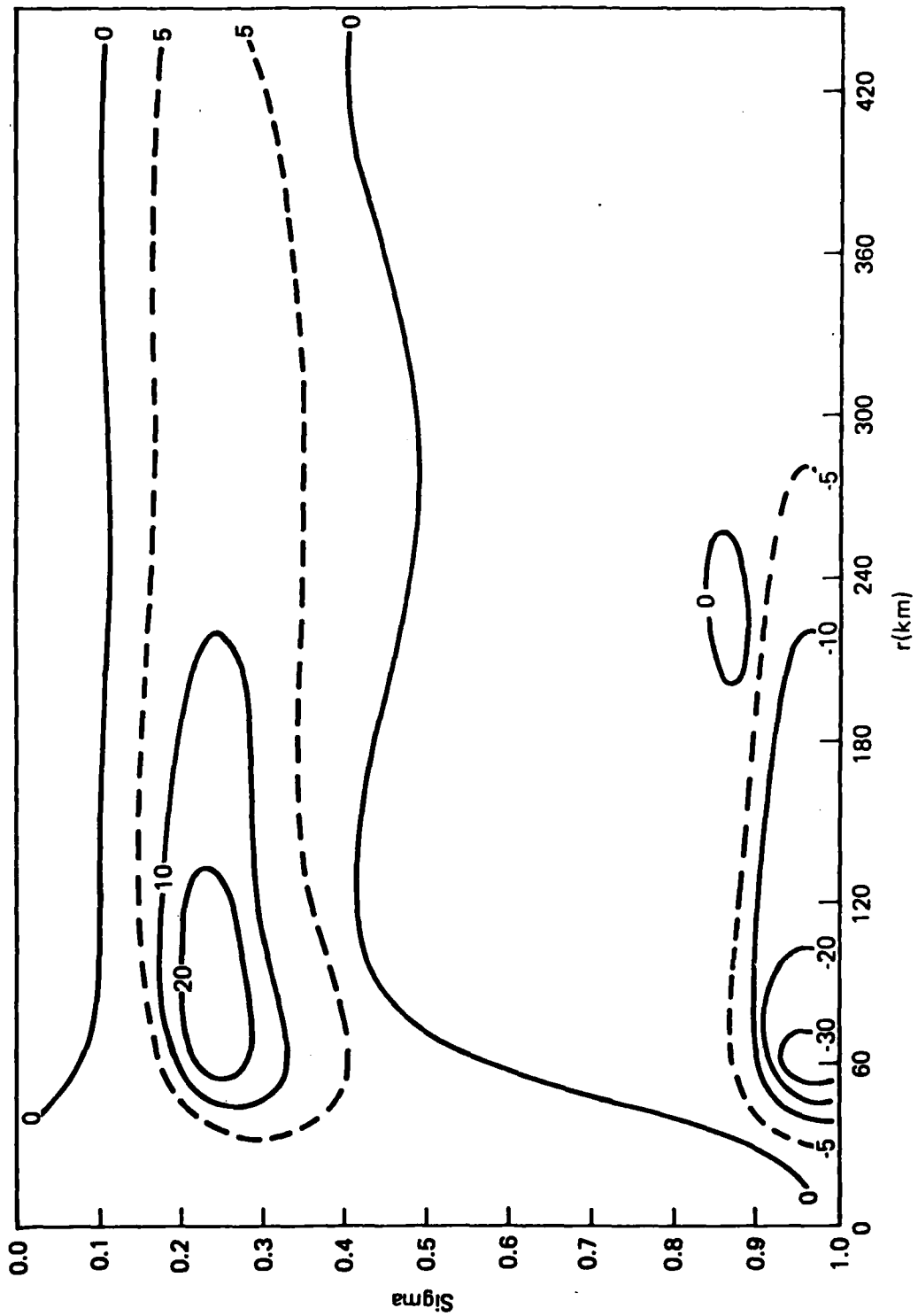


Figure 8

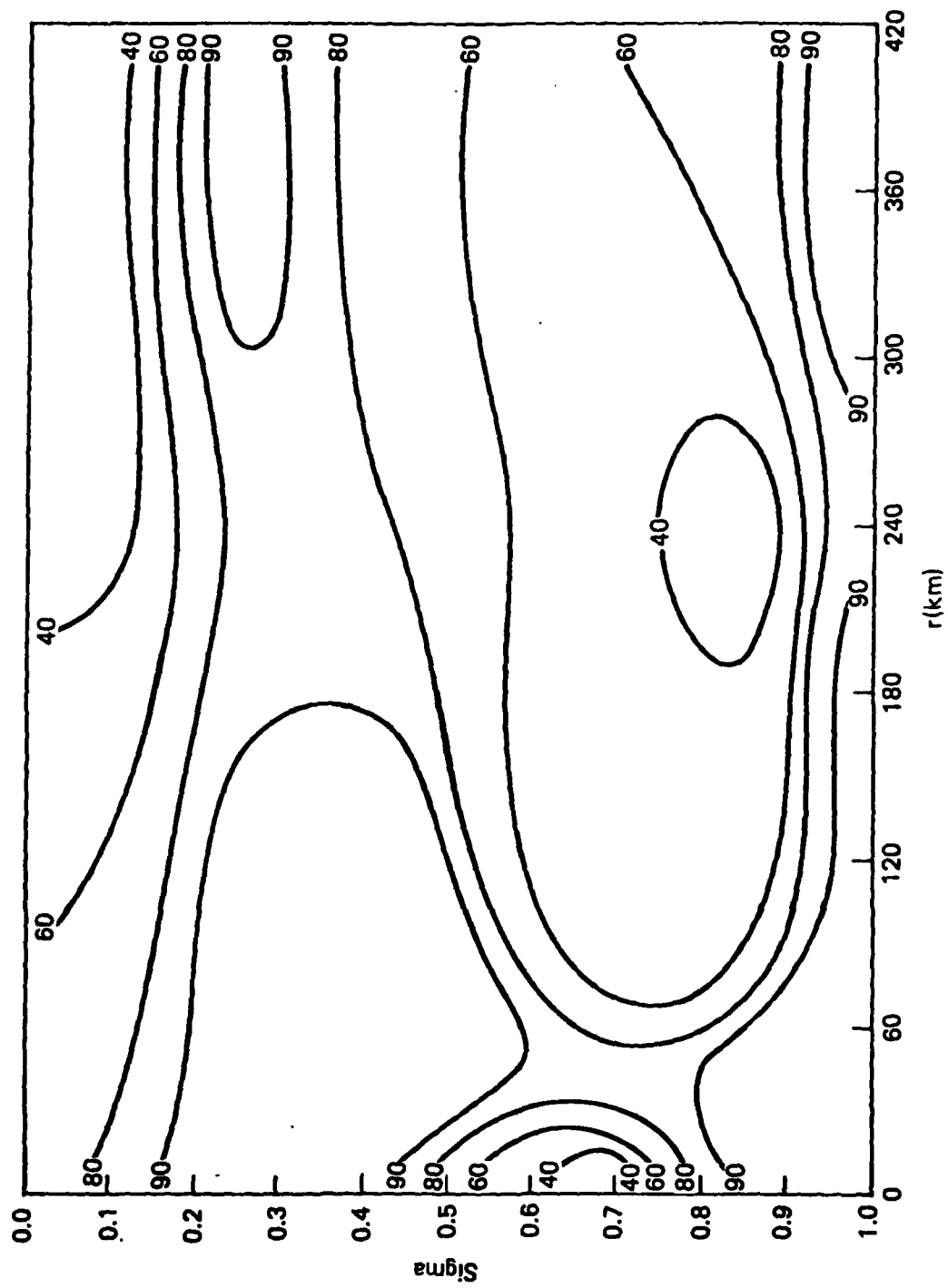


Figure 9

(844)
7/11-4-2

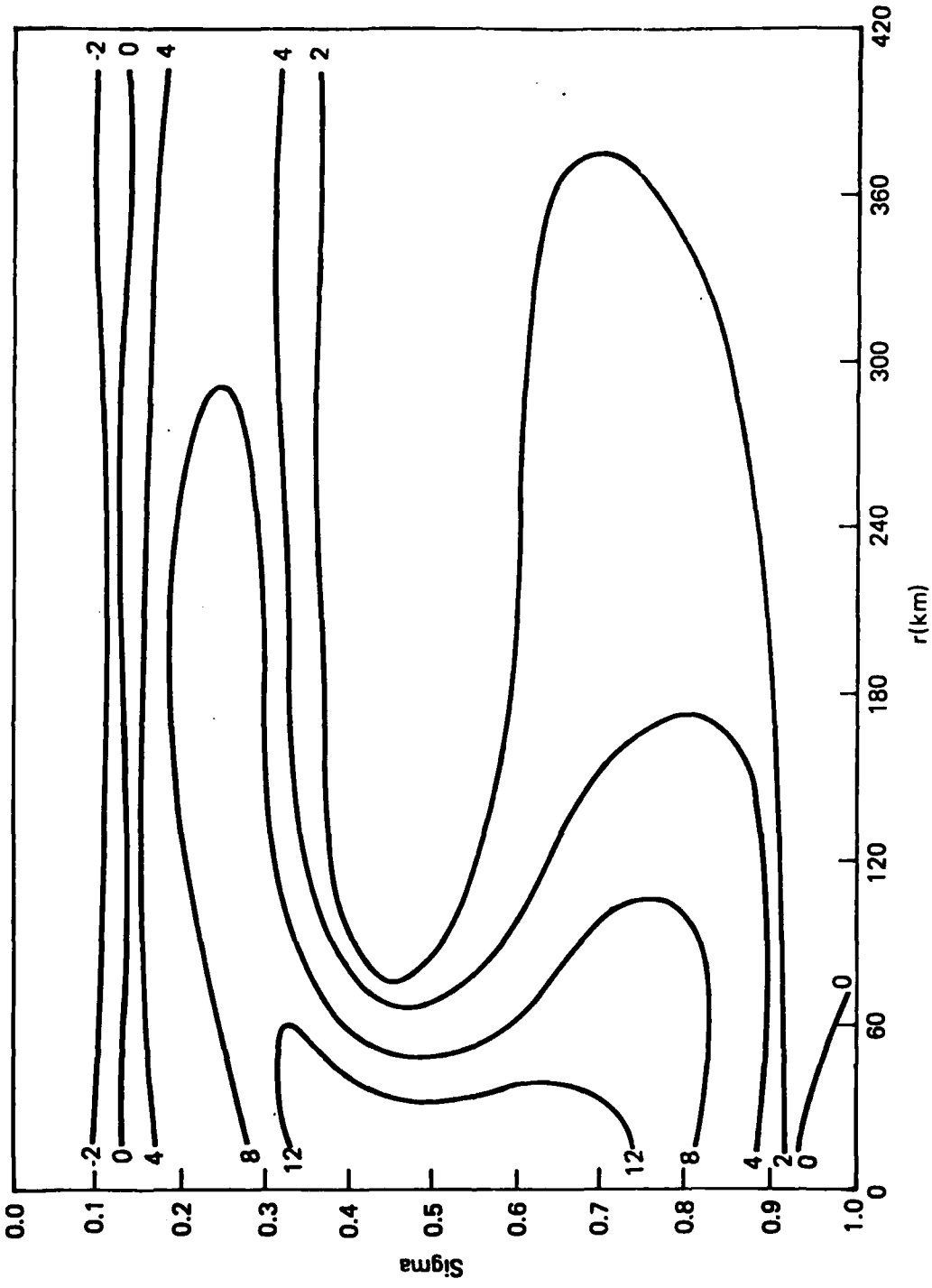


Figure 10

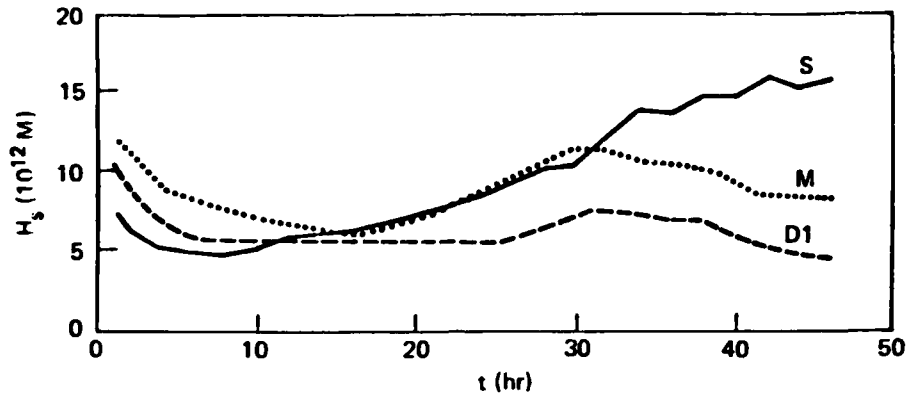


Figure 11

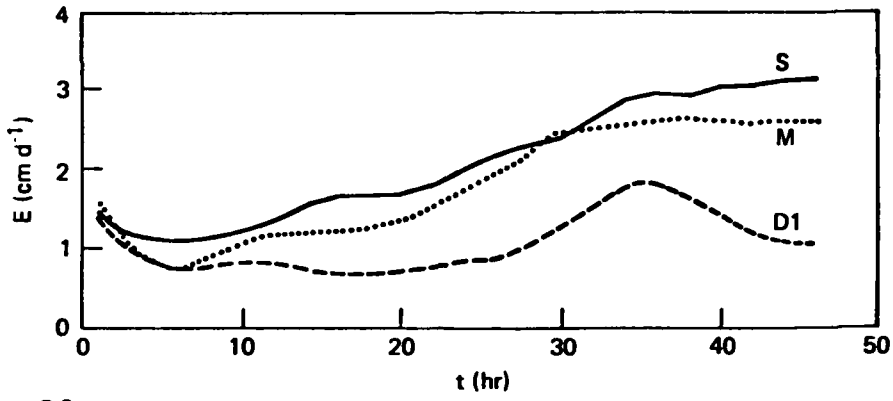


Figure 12

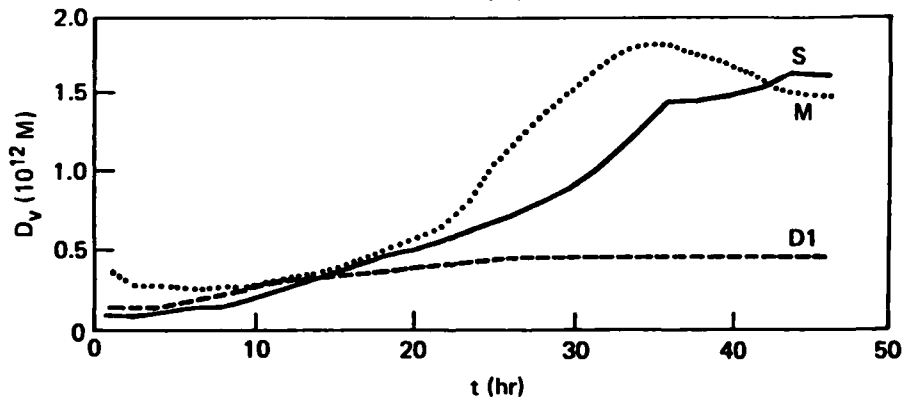


Figure 14

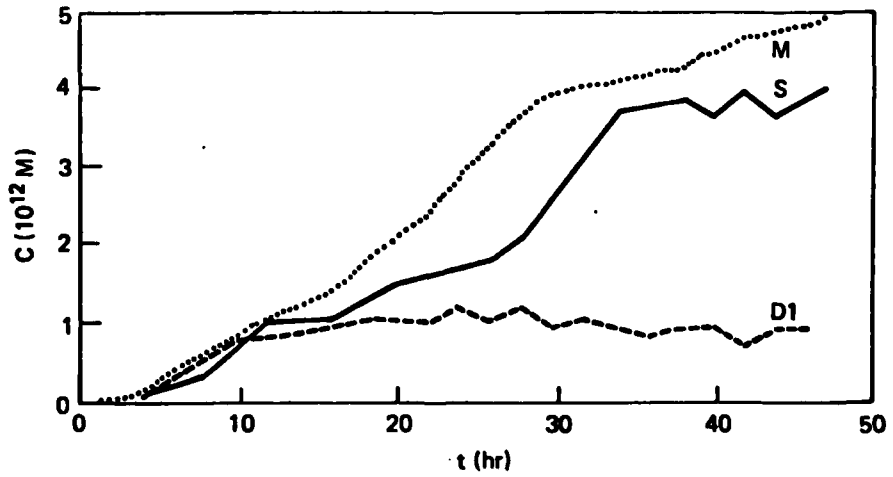


Figure 13